Discovery of a New Dimming Effect Specific to Supernovae and Gamma-Ray Bursts

Thomas B. ANDREWS
Brooklyn, NY
tba@xoba.com

June 27, 2009

Abstract

Because type Ia supernovae (SNs) are anomalously dimmed with respect to the flat ($q_o = 0.5$) Friedman Expanding Universe model, I was surprised to find that the brightest cluster galaxies (BCGs) are not anomalously dimmed. Based on the absence of anomalous dimming in BCGs, the following conclusions were reached:

- Since the light from the SNs and BCGs traverses the same space, the current hypothesis of an accelerated expansion of the universe to explain the anomalous dimming of SNs is disproved.
- The cause of the anomalous dimming must be specific to the SNs.

The first conclusion is important since current research in dark energy and the cosmological constant was initiated based on the accelerated expansion hypothesis. The disproof of this hypothesis, therefore, casts serious doubts on the existence of dark energy and the cosmological constant.

The second conclusion indicates that the occurrence of anomalous dimming depends on a basic difference between the SNs and BCGs. The only difference besides the obvious - that SNs are exploding stars and the BCGs are galaxies - is that the light curves of the SNs are limited in duration. Due on this difference, I discovered that SNs light curves are broadened at the observer by a new Hubble redshift effect. Since the total energy of the light curve is then spread over a longer time period, the apparent luminosity is reduced at the observer, causing the observed anomalous dimming of SNs.

I also show that BCGs are not anomalously dimmed because their absolute luminosity is approximately constant over the time required for the light to reach the observer.

The above conclusions also apply to Gamma Ray Bursts (GRBs) since gamma-ray "light" curves are limited in duration.

Finally, the light curve broadening effect can be used to determine if the universe is expanding or static. In the expanding universe model, a light curve broadening effect is predicted due to time-dilation for the SNs, GRBs and BCGs. Consequently, if the universe is expanding, two light curve broadening effects should occur for the SNs and GRBs. However, if the universe is static, only one light curve broadening effect will occur for the SNs and GRBs.

Fortunately, Golhaber has measured the width's of SNs light curves and conclusively showed that only one light curve broadening effect occurs. Consequently, the expanding universe model is logically falsified.

Contents

1 Introduction

Because type Ia supernovae (SNs) are anomalously dimmed with respect to a flat ($q_o = 0.5$) Friedman Expanding Universe model, it was a surprise to find that the brightest cluster galaxies (BCGs) are not anomalously dimmed. Recently, I found that gamma-ray bursts (GRBs) are also anomalously dimmed.

Anomalous dimming for the SNs and GRBs and the absence of anomalous dimming for BCGs is shown by the Hubble diagrams plotted in Figures 1, 2, 3 and 4. Although the possibility exists that luminosity evolution of the BCGs (brighter in the past) could mask the anomalous dimming of the BCGs, it is proved that BCGs do not evolve in luminosity. Therefore, the absence of anomalous dimming in BCGs appears to be a real effect.

Based on the absence of anomalous dimming in BCGs, the following conclusions were reached:

- Since the light from the SNs, GRBs and BCGs traverses the same space, the current hypothesis of an accelerated expansion of the universe to explain the anomalous dimming of SNs is disproved.
- The cause of the anomalous dimming must be specific to the SNs and GRBs.

The first conclusion is important since current research on dark energy and the cosmological constant was first initiated [1] based on the hypothesis of an accelerated expansion of the universe. The disproof of this hypothesis, therefore, casts serious doubts on the continued validity of these areas of research.

The second conclusion indicates that the occurrence of anomalous dimming depends on some basic difference between SNs and GRBs as a class and BCGs. The only difference besides the obvious - that one class represents stars and the other represents galaxies - is that the light curves of SNs and GRBs are limited in duration.

From a theoretical derivation of the anomalous dimming effect in section 4, I found that the short duration of the light curves of the SNs and GRBs results in the broadening of the light curves at the observer. Broadening occurs because the range of the Fourier frequency components of the SN light curve is narrowed by the Hubble redshift. Then, the inverse relation between the width of a light curve (represented by a rectangular pulse) and the range of the Fourier frequencies produces a broadened light curve at the observer. Since the broadened light curve spreads the total energy of the light curve at the supernova over a longer time at the observer, the apparent luminosity is reduced. This, I submit, explains the anomalous dimming of SNs and GRBs.

To understand the above observations, much depends on the non-evolution of the BCGs. The fact that the regression line in Figure 3 for the BCGs from Different Observers (see references in Appendix) is nearly straight and does not curve to the right, indicates the BCGs were not brighter in the past and thus do not evolve in luminosity.

The case for non-evolution of the BCGs from Collins and Mann [2] is more complicated. The black regression line for the observations curves to the right and thus shows what appears to be luminosity evolution. But, since the BCGs from Different Observers are observed mainly in the B band and the BCGs from Collins and Mann are observed in the K band, this is the opposite of what is expected. Assuming the expanding universe model, the luminosity evolution should be significantly larger in the B band. Thus, this anomaly indicates that some other factor is responsible for the regression line curving to the right.

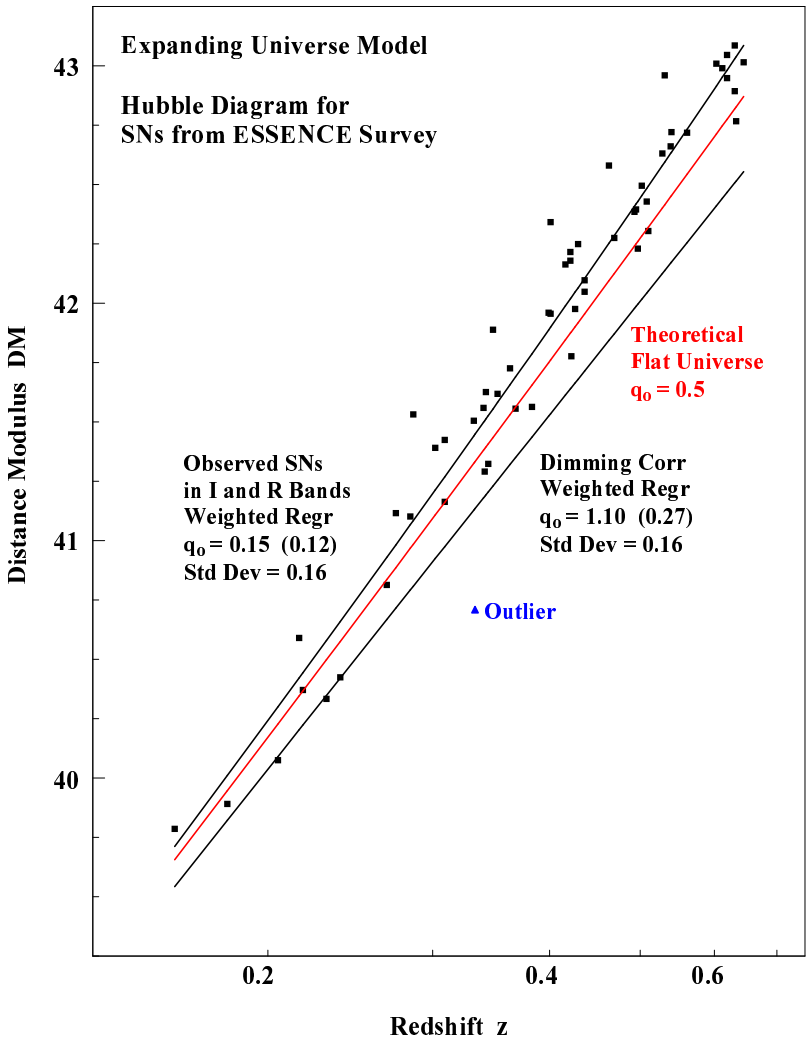

Figure 1: SNs from the ESSENCE Survey are shown in a Hubble Diagram, assuming the expanding universe model. The black squares represent the observations of the distance modulus. The blue diamond represents an outlier. The black line (on the left) represents the least squares regression for the observations. The red line represents the Friedman flat expanding universe model with $q_o = 0.5$. The second black line (on the right) represents the dimming corrected observations, DM*, calculated by subtracting 2.5 log(1 + z) from each observation.

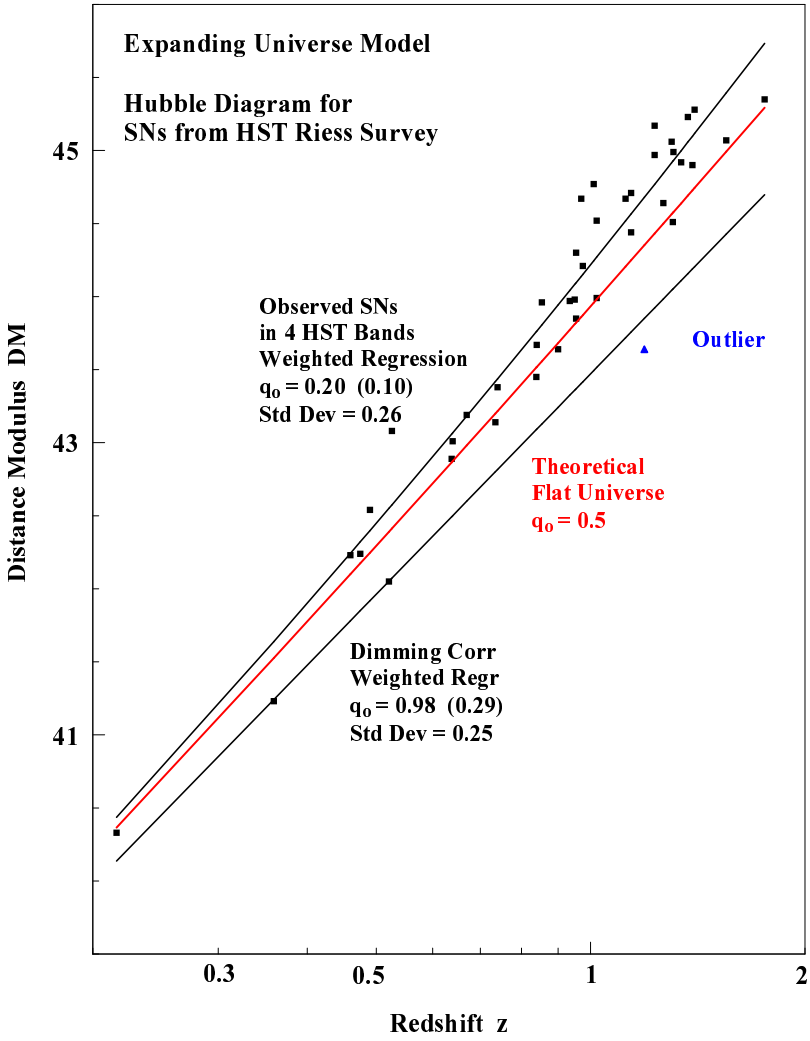

Figure 2: SNs from the HST are shown in a Hubble Diagram, assuming the expanding universe model. The black squares represent the observations of the distance modulus. The blue diamond represents an outlier. The black line (on the left) represents the least squares regression for the observations. The red line represents the flat Friedman expanding universe model with $q_o = 0.5$. The second black line represents the dimming corrected observations, DM*, calculated by subtracting 2.5 log(1 + z) from each observation.

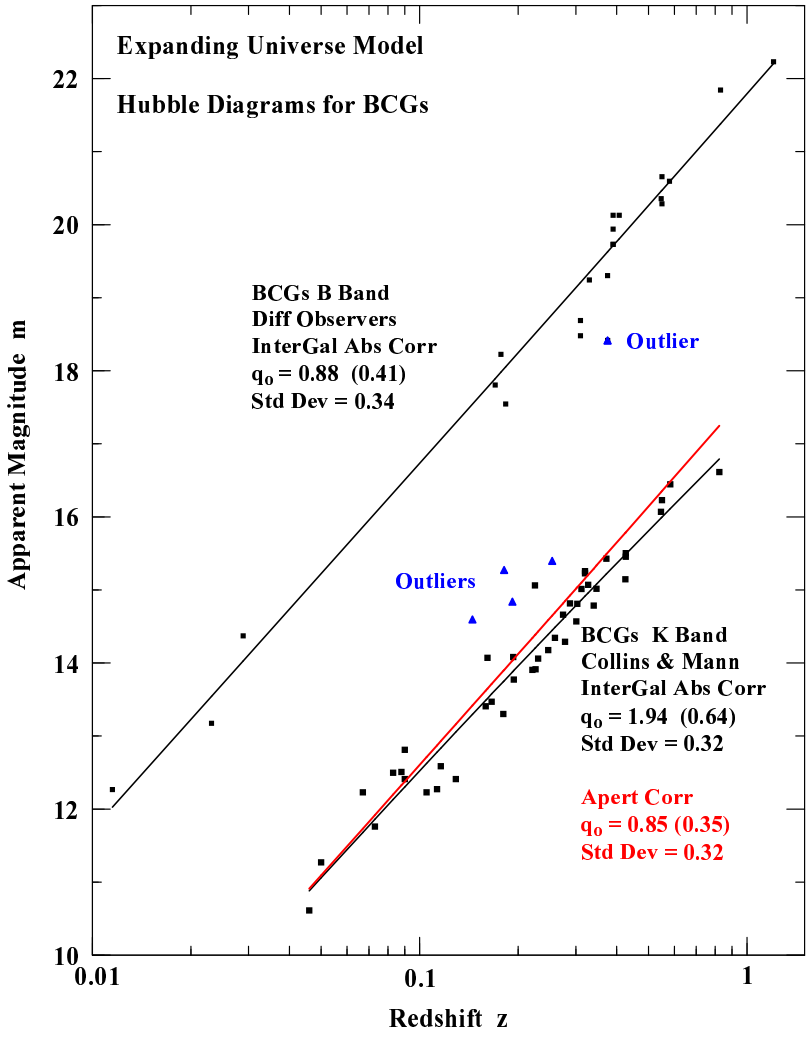

Figure 3: Two sets of BCGs, one from Different Observers and the other from Collins and Mann are shown in a Hubble Diagrams, assuming the expanding universe model. The black squares represent the observations and the blue diamonds represent outliers. The black lines are the least squares regressions for the observations. The red line is the least squares regression for the aperture corrected observations for the BCGs from Collins and Mann.

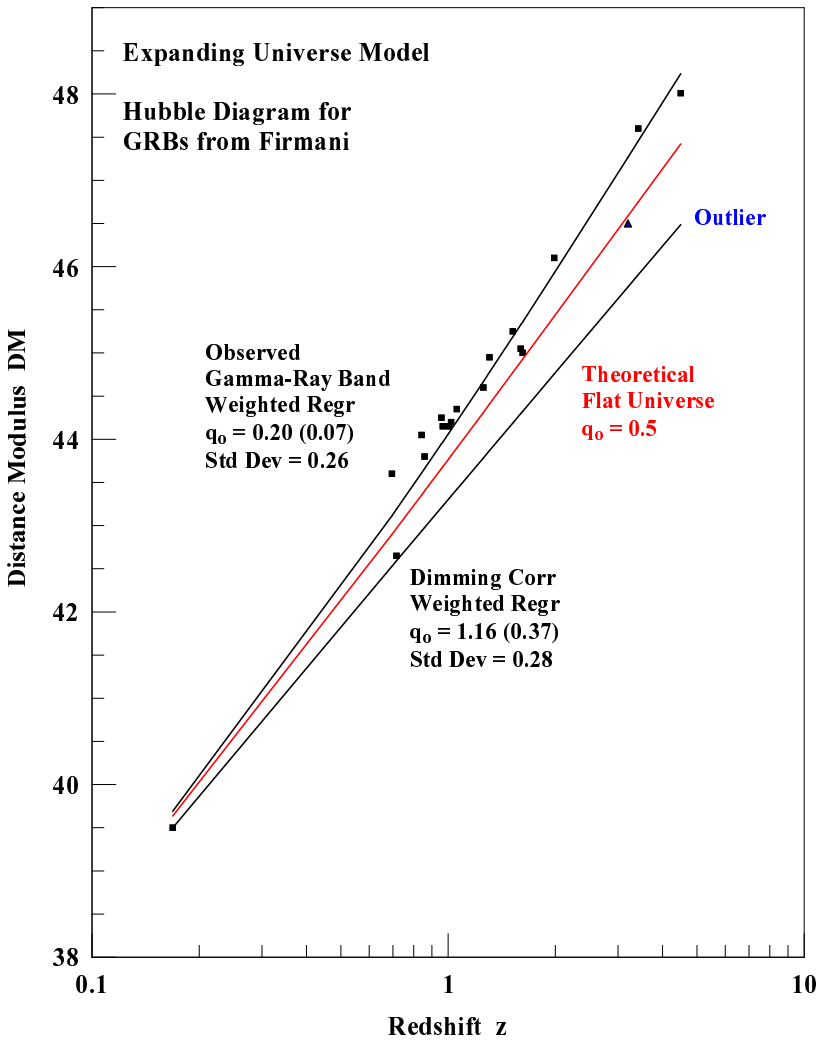

Figure 4: GRBs from Firmani are shown in a Hubble diagram assuming the expanding universe model. The black squares are the GRB observations and the single blue diamond represents an outlier. The black line (on the left) is the least square regression for the observations. The red line is the expected relationship for the flat Friedman expanding universe model. The second black line is the least squares regression for the dimming corrected observations, DM*, calculated by subtracting 2.5 log(1 + z) from each observation.

There is a significant difference between the observations of the two sets of BCGs. For the BCGs from Different Observers, the effective angular radii of BCGs were measured and the apparent magnitudes were measured within these effective angular radii. For the BCGs from Collins and Mann, the effective angular radii were not measured. Instead, apparent magnitudes were measured within angular radii calculated for a physical radius of 25 Kpc, assuming the (flat) Friedman expanding universe model with $q_o = 0.5$ and $H_o = 50$ km/sec/Mpc. Note: Because the physical radius of the BCGs entered into the measurement of the apparent magnitudes, the measurements of the apparent magnitudes of the BCGs from Collins and Mann are dependent upon the expanding universe model. In contrast, the apparent magnitudes of the BCGs from Different Observers are independent of the cosmological model.

Anticipating another conclusion of this paper - that the universe is static - the angular radii of the BCGs from Collins and Mann were recalculated assuming the static universe model for a physical radius of 25 Kpc, also with $H_o = 50$ Km/sec/Mpc. Then, assuming all BCGs in the sample have an effective radius of 38 Kpc, corrections to the apparent magnitudes for the static universe model were calculated. This angular aperture correction method is the same as used by Sandage [3]. Because the angular radii are smaller in the static universe model than in the expanding universe model, the apparent magnitudes are larger (dimmer) in the static universe model than the expanding universe model.

The red regression line shows the results of correcting the apparent magnitudes to the angular radii in the static universe model. Then, the deceleration constants, q_o, of the two BCG sets are nearly the same. From this, I conclude that the apparent luminosity evolution of the BCGs from Collins and Mann is an artifact of the expanding universe model.

In Section 6, I prove using a different logical argument that BCGs do not evolve in luminosity.

In the following sections, the observational data is described and analyzed and the anomalous dimming effect is derived. Significantly, the explanation of the anomalous dimming effect leads to the falsification of the expanding universe model. Then, the universe must be static. A static universe is also confirmed by quantitative tests of the surface brightness and the angular sizes of the BCGs from Different Observers.

2 Observations

Initially, a simple comparison of one set of SNs and one set of BCGs lead to the conjecture that the short duration of the SNs light curves and the subsequent broadening of the SNs light curves is the cause of the anomalous dimming of SNs. Although the derivation of the dimming effect in Section 4 proved this conjecture, more observational data is required to further substantiate the initial comparison. With this in mind, I expanded the observations to two set of SNs, two sets of BCGs and one set of GRBs.

2.1 Type Ia Supernovae

Type Ia supernovae are believed caused by thermonuclear explosions of carbon-oxygen white dwarfs in a binary system. The process involves mass transfer to the white dwarf from a companion star. When the white dwarf reaches the Chandrasekhar mass, the explosion occurs. Since the explosions occur at the same mass, the explosions should b nearly identical in energy release. Therefore, luminosity evolution should not occur since the physics of

thermonuclear explosions should be the same in the past. Consequently, SNs should be good standard candles.

Two recently observed (reported in 2007 and 2006) sets of Type Ia supernovae (SNs) cover nearly the entire range of redshifts which can be observed. The medium redshift set is from the ESSENCE Survey [4] which consists of 60 SNs within the redshift range 0.15 to 0.7. This survey was designed for consistency and accuracy and, therefore, uses the same methods for measuring each SNS. Photometric measurements were made by the ground based 4-meter telescope of the Cerro Tololo Inter-American Observatory. Measurements were made in the I and R bands. The highest redshift at which SNs could be measured in these bands, given the accuracy required, is about 0.7. To measure redshifts and confirm the supernovae are type Ia SNs, spectra of the SNs were observed using 8 meter or larger ground telescopes and the HST. The light curves were analyzed by the filter MLCS2k2 modified by a "glosz" prior on the extinction and color. Also, the distance modulus errors were simulated by the ESSENCE team for different priors. For the glosz prior, the observed distance modulus is slightly less than the true distance modulus beyond z = 0.6. At z = 0.7, the error reaches -0.04 magnitudes. For previously used priors, the errors start at z = 0.4 and reach -0.4 magnitudes at z = 0.7.

The second set of SNs [5] is the high redshift set where the SNs are exclusively detected and observed using the Hubble Space Telescope (HST). This survey includes an earlier set of high redshift SNs [6]. The entire program is referred to here as the HST Riess set. Because ground based telescopes suffer from excessive signal to noise ratios at high redshifts, the HST is required for observations at high redshifs. The HST can observe SNs up to approximately redshift 1.6 but begins to suffer from inaccuracies at about redshift 1.4. Observations were made in four HST bands which were K-Corrected to the U, B and V bands.

Observations of the HST set were analyzed by the same filter, MLCS2k2, as in the ESSENCE set but the priors on extinction and color are different. The resultant sample is divided into "gold" and 'silver' sets. The gold set are those definitely proved to be type Ia SNs and whose photometric record gave a robust distance estimate. The silver set are those with one defective measurement either in the photometric or the spectral record. Those SNs with more than one defective measurement were deleted. In the analysis here, I use both the gold and silver set since my analysis shows no difference statistically between the gold and silver observations.

2.2 Brightest Cluster Galaxies

There are major advantages in using BCGs to measure cosmological distances. First, the BCGs are known as good standard candles at low redshifts. At high redshifts, luminosity evolution of the BCGs is widely thought to occur. Nevertheless, I prove based on observational data that BCGs (as a class) do not evolve in luminosity. This justifies using BCGs as standard candles at high redshifts. Second, since BCGs are nearly the same absolute luminosity (standard deviation 0.3 magnitude), the observational data is independent of a specific cosmological model. These two features of BCGs justify using BCGs as standard candles at high redshifts.

Two sets of BCGs are used. In the first set, most of the BCGs were found in Fundamental Plane Studies of elliptical galaxies in clusters by different groups of observers. Therefore, the first set is labeled "from Different Observers" (see references in the Appendix). All of the BCGs were observed using the HST except the two lowest redshift BCGs which were observed by ground telescopes. In all cases, the average surface brightness was measured

within the effective (half light) radius using very similar methods. Furthermore, all redshifts were spectroscopically determined. Most observations were measured in the B band. Measurements in other bands were converted to the B band using conversion factors from Fukugita [11].

The second set of BCGs is from Collins and Mann [2]. The primary reason for including this set was to prove that luminosity evolution does not occur by comparing the Hubble diagrams of the two sets of BCGs. The clusters are X-ray selected and, consequently, are more likely at high redshifts to represent bona fide clusters than for optically selected clusters. The BCGs were observed in the K band using a ground based telescope. Apparent magnitudes were measured within an aperture corresponding to a physical radius of 25 Kpc calculated assuming the Friedman expanding universe model with $q_o = 0.5$ and $H_o = 50$ Km/sec/Mpc. The apparent magnitudes were only corrected for galactic dust absorption.

2.3 Gamma-Ray Bursts

The Gamma-Ray Bursts (GRBs) set was added primarily to show GRBs are anomalously dimmed the same as SNs and for the same reason - their short duration light curve. The set of GRBs is from Fermani et al [7]. Since GRBs are the brightest explosions in the universe, they can be observed at much higher redshifts than SNs. However, their absolute luminosity varies much more than SNs. Thus, like SNs but to a greater degree, this requires methods for determining their absolute luminosity. Since various properties of their bursts have been found to correlate with their absolute luminosity, significant progress has been made in turning them into standard candles. However, the accuracy of the distance measurements still remains less than SNs.

The 19 GRBs in the set are the only long GRBs which have both redshifts and sufficient observations for prediction of the absolute magnitudes. Based on the recent discovery of a tight correlation [8] between the energetics and other prompt γ-ray emission properties of GRBs, Fermani has developed reasonably accurate distance measurements for this set of GRBs.

2.4 Corrections to Observations

The BCGs observational data was corrected by several methods. Both sets of BCGs were corrected for inter galactic dust absorption [10]. The full absorption (predicted assuming a constant dust density) was applied in full to B band observations but only half the absorption was applied to observations in longer wavelength bands where dust has less effect. Thus, in the BCGs from Different Observers, the full absorption was applied to BCGs measured in the B band and half to measurements in longer wavelength bands. For the K band observations of Collins and Mann, half the full absorption was applied to all the observations. In any case, the corrections were small with the largest only 0.14 magnitudes for a BCG from Different Observers at redshift 1.2. The intergalactic dust absorption corrections were not applied to the SNs since their methods for measuring dust absorption in the host galaxies presumably also measure the intergalactic dust absorption.

In addition, for the BCGs from different observers, the Fundamental Plane method was used to normalize the luminosity to BCGs with a fixed effective radius of 38 Kpc. This method is based on an accurate linear relation between the surface brightness and the logarithm of the effective radius of elliptical galaxies.

As previously described, the Collins and Mann observed apparent magnitudes were aperture corrected to the static universe model. I also applied K-Corrections obtained from Aragon-Salamanca [12] to the observations. Finally, since the observations of Collins and Mann were made using a ground telescope, small corrections for "seeing" from Saglia [13] were made.

The observational data for all the data sets and their calculated parameters are listed in the Appendix.

3 Analysis of Observations

Table 1 below shows the least squares Hubble diagram parameters for SNs, BCGs and GRBs assuming the Friedman expanding universe model (without the cosmological constant) given by

$$m = M + 5\log q_o^{-2}[q_o z + (q_o - 1)(-1 + \sqrt{(1 + 2q_o z)})] + C. \quad (1)$$

In the above equation, m is the apparent magnitude, M is the absolute magnitude, q_o is the deceleration parameter, z is the Hubble redshift and C is a constant. Alternatively, instead of m, the distance modulus, DM = m - M may be used.

TABLE 1
Hubble Diagram Parameters for SNs, BCGs and GRBs
Assuming the Friedmann Expanding Universe Model

	#	Outliers	q_o	Constant	Std Dev
SNs ESSENCE Survey	60				
Observed		1	0.15 (0.12)	43.57 (0.07)	0.16
Dimming Corr		1	1.10 (0.27)	43.55 (0.09)	0.16
SNs HST from Riess	41				
Observed		1	0.20 (0.10)	43.59 (0.09)	0.26
Dimming Corr		1	0.98 (0.29)	43.46 (0.16)	0.25
GRBs Firmani	19				
Observed		1	0.15 (0.06)	43.33 (0.10)	0.26
Dimming Corr		1	1.02 (0.24)	43.28 (0.16)	0.26
BCGs Diff Observers (InterGal Abs Corr)	22				
Observed		1	0.88 (0.41)	21.72 (0.14)	0.34
Fund Plane Corr		0	1.16 (0.35)	21.80 (0.11)	0.26
BCGs Collins & Mann (InterGal Abs Corr)	47				
Observed		4	1.94 (0.64)	17.61 (0.11)	0.32
Aperture Corr		4	0.85 (0.35)	17.59 (0.09)	0.32

In Table 1, the deceleration parameters of the observed SNs and GRBs are positive between 0.15 and 0.20 while the deceleration parameters of the BCGs are close to 1. Since deceleration constants for SNs determined from earlier surveys, primarily in the 1990's, were negative, it must be concluded that the results of earlier surveys were biased by systematic errors. This conclusion is based on the much better coverage and measurement of the SNs light curves by current surveys and the more accurate analysis of the light curves. The measurement of dust absorption in the host galaxy by the earlier surveys is a likely source of those systematic errors. The new positive estimates of the deceleration parameter also tend to invalidate the hypothesis of an accelerated expansion of the universe.

In contrast, the deceleration constants for the dimming corrected SNs and GRBs are close to 1. The dimming corrected observations, DM*, are calculated by subtracting

2.5 log(1 + z) from the DM observations. The correction factor is equal to the theoretical anomalous dimming factor determined in Section 4 (see equation 11). Consequently, the DM* are equivalent to the apparent magnitudes, m, of the BCGs since both show no anomalous dimming. In fact, the dimming corrected q_o values of the SNs and GRBs and the q_o values of the BCGs are found to cluster around 1 instead of the expected 0.5 for a flat expanding universe. This appears to be an anomalous result but is not because a q_o of approximately 1 corresponds to a flat static universe. Therefore, If the universe is actually static, a $q_o \approx 1$ is the expected result.

4 Derivation of the Anomalous Dimming Effect for Type Ia Supernovae and Gamma-Ray Bursts

To derive the anomalous dimming effect for SNs and GRBs, consider a single wave of limited duration, a, in the rest frame of the supernova along with the observer at a distance, l, from the supernova. The equation of the wave is represented by the equation

$$y(x) = A \ \sin(\omega_m x/c) \tag{2}$$

with A = 1 for $0 \geq x \leq a$ and A = 0 for $a < x \leq l$. This limited duration wave is shown in the rest frame of the supernova in the first panel of Figure 5.

The wave represents just one of the many spectral frequencies produced by atoms in the supernova. The limited wave then propagates on a simulated string of length $l >> a$. (Note: the reduction in the apparent luminosity by the inverse square law is neglected in this derivation). Admittedly, the representation of the light curve by a single frequency rectangular waveform is a crude approximation for the actual light curve; nevertheless, the rectangular waveform of the light curve correctly represents the underlying physics.

To determine the waveform of the supernova at the observer, a Fourier analysis of the supernova light curve appears the best method to use. Similar problems are successfully solved by Fourier analysis, for example, the change in shape with distance of a waveform in a dispersive medium. To solve this particular problem, the waveform is first represented by a sum of Fourier frequencies. Then, each of the Fourier frequencies is propagated at it's own characteristic velocity. Finally, adding together these Fourier components at a later time, the change in the original waveform due to the dispersion of the medium can be exactly determined.

Thus, adopting the Fourier method, the limited duration light curve of the supernova in equation 2 is represented by a Fourier normal modes expansion [14] over the length of the string given by

$$y(x) = \sum_{n=1}^{\infty} b_n \sin(\omega_n x/c) \tag{3}$$

where b_n is the amplitude of the nth sinusoidal term and the ω_n are the Fourier normal mode frequencies. The b_n are given by

$$b_n = \frac{2}{l}\int_0^l y(x)\sin(\omega_n x/c)\ dx = \frac{2}{l}\int_0^a A\ \sin(\omega_m x/c)\sin(\omega_n x/c)dx \tag{4}$$

where a is the duration of the sinusoidal pulse.

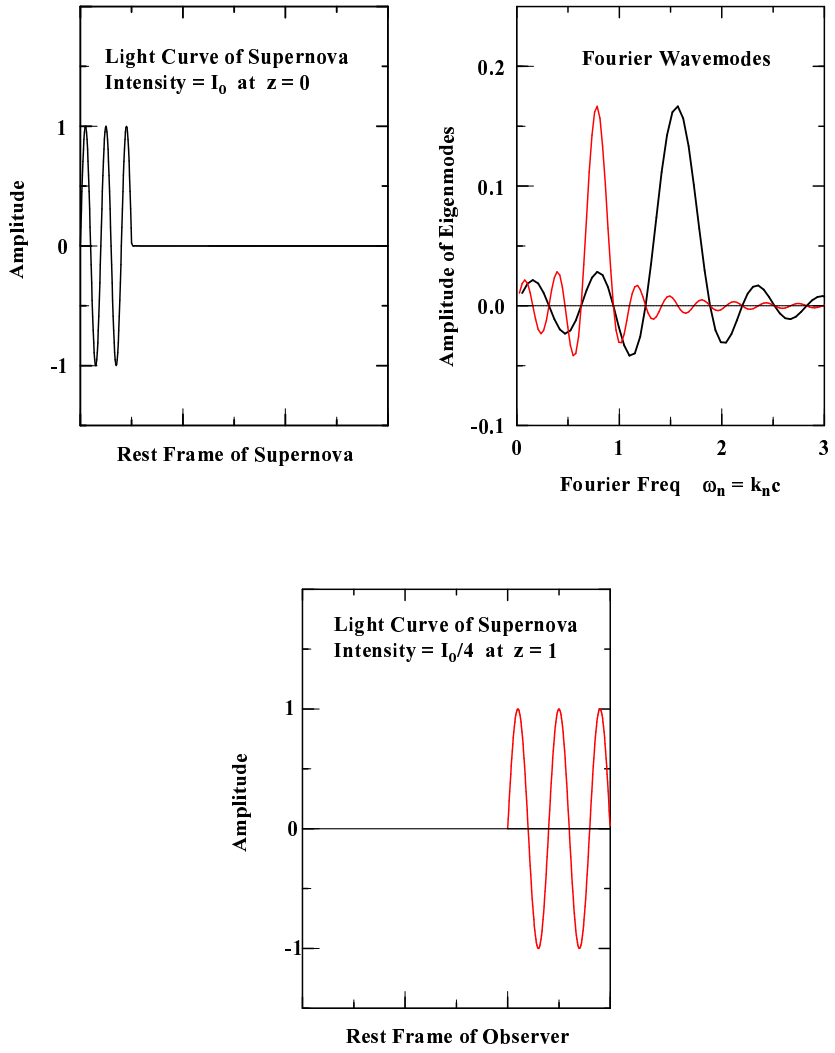

Figure 5: The Fourier analysis of a supernova light curve is illustrated in the above three panels: The first panel represents the light curve of a supernova by a rectangular pulse with a single sinusoidal frequency. In the second panel, the black line represents the amplitudes of the Fourier wavemodes at z = 0. The red line represents the amplitudes of the Fourier wavemodes redshifted to z = 1 at the observer. In the third panel, the red line shows the light curve redshifted to z = 1 at the observer with the light curve width doubled.

In order to integrate equation 4, the sin terms are first transformed to cos terms involving the sum and difference frequencies, giving

$$b_n = \frac{A}{l}\int_0^a [\cos((\omega_m - \omega_n)x/c) - \cos((\omega_m + \omega_n)x/c)]dx. \tag{5}$$

Integrating, the amplitudes are given by

$$b_n = A\frac{c}{l}\left(\frac{\sin((\omega_m - \omega_n)a/c)}{(\omega_m - \omega_n)} - \frac{\sin((\omega_m + \omega_n)a/c)}{(\omega_m + \omega_n)}\right). \tag{6}$$

The amplitudes, b_n, of the Fourier normal mode frequencies calculated from equation 6 are shown in the second panel of Figure 5. The solid line represents the amplitudes of the Fourier normal modes frequencies at the supernova. The red line represents the Fourier amplitudes, b'$_n$, Hubble redshifted to z = 1 at the observer.

In the third panel of Figure 5, the supernova light curve at the observer, y'(x), is reconstituted from the redshifted Fourier modes using the equation

$$y'(x) = \sum_{n=1}^{\infty} b_n \sin(\omega'_n x/c) \tag{7}$$

where the b_n are the Fourier wave amplitudes calculated for the initial limited duration wave at the supernova and $\omega'_n = \omega_n/(1+z)$.

Then, assuming z =1 at the observer, the supernova light curve, y'(x), is doubled in width. The theoretical dimming factor is determined next.

A general feature of a Fourier analysis [15] of a waveform is the inverse relation between the frequency range of the significant Fourier frequencies and the width of the waveform. A narrow waveform implies a wide range of Fourier frequencies while a wide waveform implies a narrow range of Fourier frequencies. This is the physical process upon which the broadening of the supernova light curve is based.

As a specific example of the inverse relationship between a and $\Delta\omega$, consider the pressure broadening of spectral lines emitted in a discharge tube. As the pressure of the gas decreases, the mean free path, a, between the collisions of atoms increases. As a result, the observed frequency range, $\Delta\omega$, of the spectral lines decreases.

At the SNs, the significant Fourier normal frequencies are within the frequency range

$$\Delta\omega = 2\pi\frac{c}{a} \tag{8}$$

around the original spectral frequency, ω_m. For a supernova light curve with an approximate duration of 2 months, $\Delta\omega \approx 3 \times 10^{-7}$ hertz.

At the observer, the Fourier normal mode frequencies are redshifted by the factor 1/(1 + z). Consequently, the frequency range of the normal mode frequencies at the observer, $\Delta\omega'$, is reduced to

$$\Delta\omega' = \Delta\omega/(1+z). \tag{9}$$

Therefore, from equation 8, the width, a', of the rectangular pulse at the observer becomes

$$a' = \frac{2\pi c}{\Delta\omega'} = \frac{2\pi c}{\Delta\omega}(1+z) = a(1+z). \tag{10}$$

Then, the apparent luminosity, l_o, of a supernova is decreased at the observer by

$$l = l_o/(1+z) \tag{11}$$

due to the broadening of the light curve by the same factor (1 + z). This reduction is in addition to the decrease in the apparent luminosity due to the Hubble redshift and is responsible for the anomalous dimming of SNs and GRBs.

Note: The anomalous dimming of SNs may be better explained in terms of the total energy (ergs) of the light curve and the apparent luminosity (ergs/cm^2/sec) at the observer. Given that the energy and apparent luminosity of the light curve at the supernova are E_o and l_o respectively, the reduction in the energy of the light curve at the observer is $E = E_o/2$ due to the Hubble redshift. Then, the apparent luminosity is reduced by an additional factor of two (at $z = 1$) by the doubling of the width of the light curve. Finally, the combined reduction in the apparent luminosity at the observer is $l = l_o/4$.

4.1 Phase Coherence of Light Over Cosmological Distances

The above derivation implicitly assumes that the Fourier frequency components retain their phase relations when the light curve is observed at the observer. Phase coherence is required since the broadening of the light curve of SNs is an interference effect.

Obviously, an observational test of phase coherence would resolve the problem. Recently, Lieu [16] has noted that an Airy ring diffraction pattern is clearly discerned from the distant source PKS 0201+113 at a redshift of $z = 3.61$. This observation clearly indicates phase coherence is present over very large distances.

5 Derivation of the Absence of the Anomalous Dimming Effect for the Brightest Cluster Galaxies

As previously noted, observations of the BCGs do not show anomalous dimming. How can this be explained? The same Fourier analysis used to derive the anomalous dimming of supernovae should be applicable.

Assume the absolute luminosities of BCGs are nearly constant during the time the light takes to reach the observer. Then, represent a BCG by a single frequency wavemode. It will be shown that only the same Hubble redshifted wavemode exists at the observer. Thus, a spread in the Fourier wavemodes does not occur.

This can be shown theoretically by considering a single frequency wavemode, given by

$$y(x) = A\ \sin(\omega_m x/c) \tag{12}$$

where $A = 1$ for $0 \geq x \leq l$. In this equation, the amplitude of the wave is constant over the distance, l, between a BCG and the observer.

Therefore, consider the equation for the Fourier amplitudes

$$b_n = \frac{2}{l}\int_0^l y(x)\sin(\omega_n x/c)\ dx = \frac{2}{l}\int_0^l A\ \sin(\omega_m x/c)\sin(\omega_n x/c)\ dx \tag{13}$$

where the integration of the right hand expression is over the distance, l, between the galaxy and the observer. Note: Compare this integration with the corresponding integration for supernova in equation 4 over the distance, a.

Since the integration is over the entire length of the string, all the b_n are zero except for the wavemodes for which $n = m$. Therefore, only one wavemode occurs at the BCG and this wavemode is identical to the initial wavemode.

Consequently, after redshifting the frequency of this wavemode, only one redshifted wavemode occurs at the observer. Therefore, no light curve broadening effect occurs at the observer, confirming theoretically the observed absence of anomalous dimming in BCGs.

The Fourier analysis of a single wavemode, similar to the analysis for supernovae, is shown in the three panels of Figure 6. Thus, an observer measures $\mathrm{l} = \mathrm{l}_o/2$ from a BCG (at $z = 1$), showing the absence of anomalous dimming for BCGs.

Note: The same arguments above also apply to the absence of anomalous dimming in ordinary galaxies.

6 Falsification of the Expanding Universe Model

However, the existence of the new light broadening effect has a broader significance. As is well known, the expanding universe model already incorporates a light curve broadening effect due to time-dilation [17]. Time-dilation occurs because photons produced at a later time have to travel a longer distance to the observer than photons produced at an earlier time in an expanding universe. Consequently, the photons at the observer are spread over a longer time interval proportional to (1 + z). This broadening produces a decrease in the apparent luminosity by the factor 1/(1 + z) for SNs.

As a result, in the expanding universe model, SNs should be subject to two light curve broadening effects, one from the time-dilation effect in the expanding universe model and the second from the new light curve broadening effect. The question then is whether or not two light curve broadening effects for SNs are observed?

This question has already been addressed by Goldhaber [18] who found that the increase in duration of the light curves for SNs versus redshift, z, corresponds to a single light curve broadening effect. The increase in the duration was determined from observations of the width factor, w, for a large set of type Ia supernovae. The measurement of w is based on fitting the K-corrected and normalized light curves of type Ia supernovae to a standard light curve for type Ia supernovae. Goldhaber's observations are listed in in the Appendix in Table 8A.

In theory, for a single light curve broadening effect, w = s(1 + z) in which, by definition, s equals 1 for a standard Type Ia supernovae light curve. Goldhaber then plotted w versus (1 + z) resulting in a slope of 1.07 with a standard deviation of 0.06. This slope confirms that only a single light broadening effect occurs.

Because of the importance of Goldhaber's result, I have also plotted his data in Figure 7 and find that the slope equals 0.98 with a standard deviation of 0.08 assuming that w = 0 at z = 0. The difference in slope is due to two outliers which are excluded from the regression calculation.

Because Goldhaber's analysis of the light curve width observations contradict the prediction of two light curve broadening effects in the expanding universe model, the expanding universe model is logically falsified.

Note: Blondin [19] has also deduced the existence of only one light curve broadening effect from the spectral aging characteristics of the SNs light curves.

7 Flat Static Universe Model

Since the expanding universe model is falsified, a static universe is hypothesized, i.e. a non expanding universe. This section shows modified Hubble diagrams of SNs, BCGs and GRBs

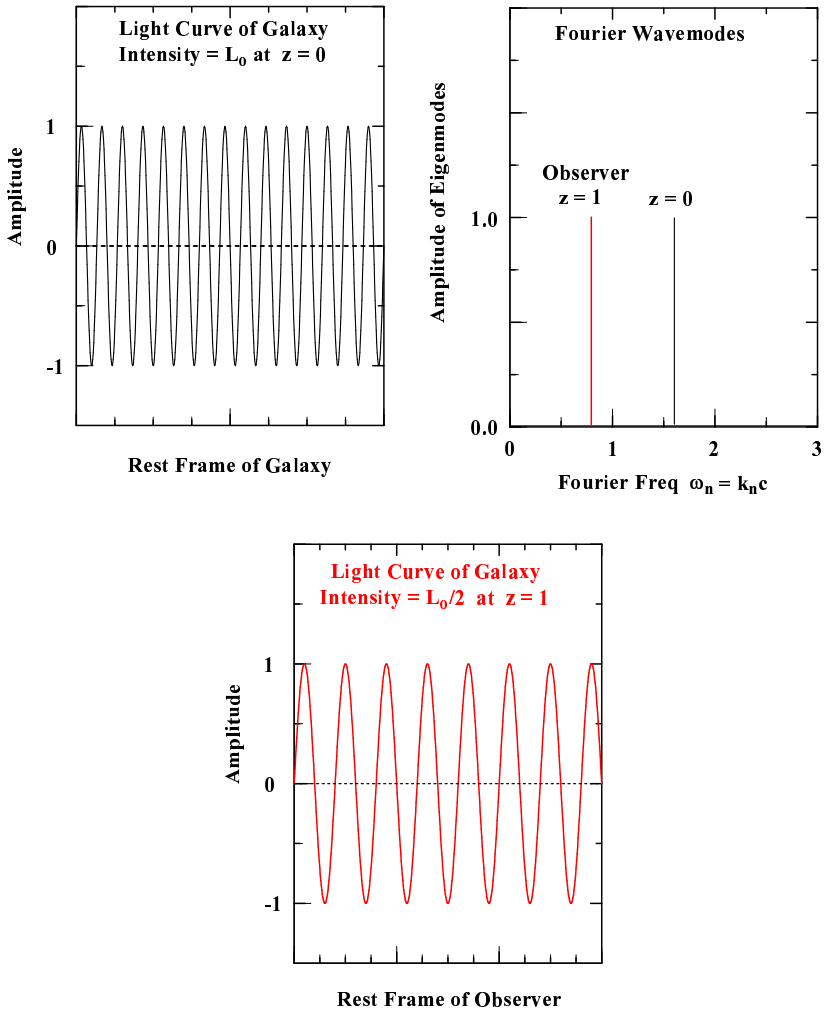

Figure 6: The Fourier analysis of a BCG with constant luminosity is illustrated in the above three panels: In the first panel, the black line represents a constant amplitude wavemode in the BCG rest frame. In the second panel, the black line represents the amplitude of a single Fourier wavemode in the BCG rest frame. The red line represents the amplitude of a single Fourier wavemode redshifted to z =1 at the observer. In the third panel, the red line represents the initial wavemode redshifted to z = 1 at the observer.

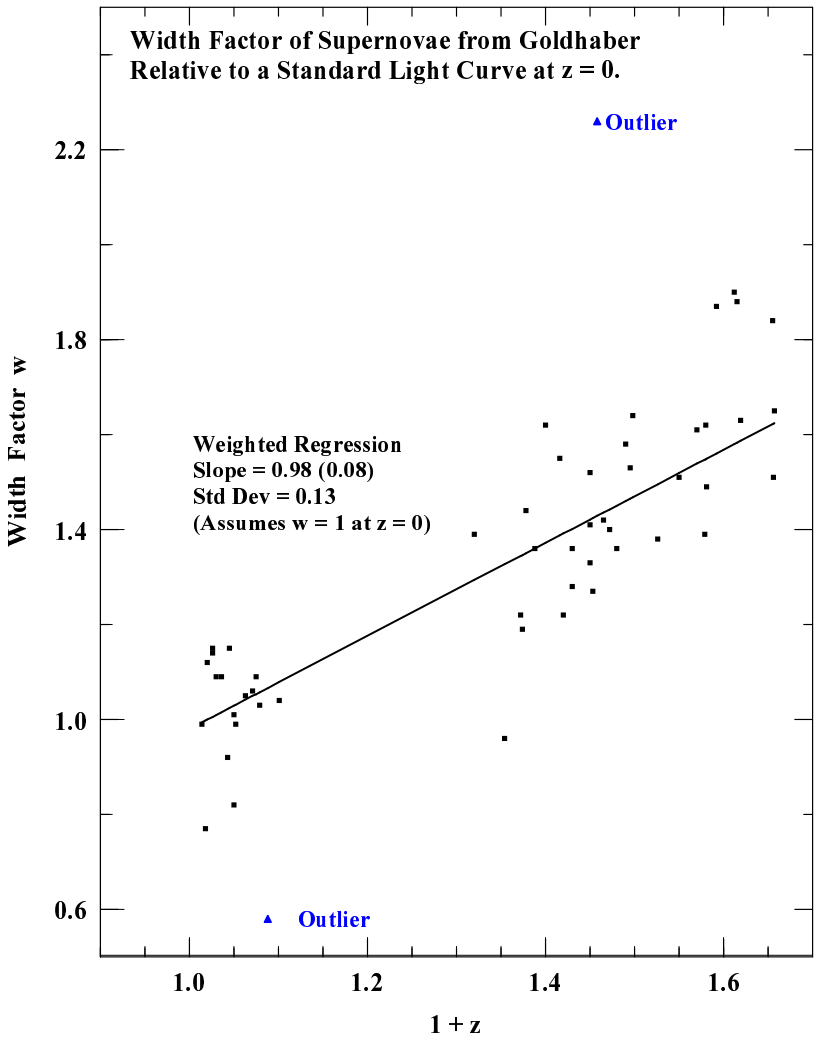

Figure 7: Widths of the light curves of Type Ia Supernovae from Goldhaber relative to a standard light curve at z = 0. The black squares represent the observations and the blue diamonds represent the outliers. A slope of one corresponds to a single light curve broadening effect.

which are consistent with a static universe. In Sections 9 and 10, surface brightness and an angular size tests of the BCGS prove conclusively that the universe is static. This provides additional confirmation that the explanation of the anomalous dimming of supernovae is correct.

In a flat static universe model, the apparent magnitude, m, is given by

$$m = M + 5\log(r) + 2.5\log(1+z) + C. \tag{14}$$

where the coordinate distance [20] r = s/R = ln(1 + z). s is the physical distance and R is the mean interactive radius of the universe. At low redshifts, r ≈ z.

In equation 14, the absolute magnitude, M, is a constant. The second term accounts for the reduction in luminosity due to the inverse square law and the third term accounts for the loss of energy due to the Hubble redshift. This equation applies directly to the BCGs. For SNs, an additional term, 2.5 log(1 + z), to account for the anomalous dimming effect must be added to the right side.

Given equation 14, a plot of the apparent magnitude versus log(r) is a curved line. However, a change in the dependent variable, replacing the apparent magnitude, m, by m - 2.5 log(1 + z) converts the curved line to a straight line. Then, equation 14 becomes

$$m - 2.5\log(1+z) = M + 5\log(r) + C. \tag{15}$$

Since this equation with m - 2.5 log(1 + z) as the dependent variable is linear, it is easier to statistically analyze and interpret observations. No appreciable loss in accuracy due to using m - 2.5 log(1 + z) as the dependent variable occurs since redshifts are more accurately measured than apparent magnitudes. With the change in the dependent variable and the use of r instead of z as the distance, the graphs are referred to as "Modified Hubble Diagrams".

7.1 Type Ia Supernovae

Figures 8 and 9 show the modified Hubble diagrams for the SNs assuming the static universe model.

For the SNs from the ESSENCE Survey, the least squares regression equation for the dimming corrected distance modulus DM* (defined as DM* = DM - 2.5*log (1 + z)) is given by

$$DM^* - 2.5\log(1+z) = 5.00\log(r) + 43.53. \tag{16}$$

Note: The theoretical dimming of supernovae is derived in section 4. The dimming is given by equation 11.

Similarly, for the SNs from the HST Survey, the least squares regression equation is

$$DM^* - 2.5\log(1+z) = 5.16\log(r) + 43.54. \tag{17}$$

Both slopes are statistically consistent with the theoretical slope of 5 for a flat static universe.

7.2 Brightest Cluster Galaxies

Figure 10 shows the modified Hubble diagram for the two sets of BCGs assuming the static universe model.

The apparent magnitudes for the BCGs from Different Observers were calculated from the observed surface brightness using the relation

$$m_e = -2.5\log(\pi\theta^2) + \mu_e \tag{18}$$

where m_e and μ_e are respectively the apparent magnitude and average surface brightness within the effective angular radius θ. Since the surface brightness observations are independent of any cosmological model, the apparent magnitudes are also independent of any cosmological model.

Then, using the apparent magnitudes, the least square regression equations for the BCGs corrected for inter galactic dust absorption are:

For the BCGs from Different Observers, for observations independent of the cosmological model,

$$m_e - 2.5 \log (1 + z) = 5.05 \log (r) + 21.78. \tag{19}$$

For the BCGs from Different Observers, corrected using the Fundamental Plane method,

$$m_e - 2.5 \log (1 + z) = 5.01 \log (r) + 21.73. \tag{20}$$

For the BCGs from Collins and Mann, with apertures corrected to the static universe,

$$m - 2.5 \log (1 + z) = 5.04 \log (r) + 17.66. \tag{21}$$

The fact that both sets of BCGs fit a straight line with a slope close to 5 is a strong indication that the BCGs do not evolve in luminosity.

7.3 Gamma-Ray Bursts

Figure 11 shows that the modified Hubble diagram for GRBs assuming the static universe model. As in the case of SNs, DM* represents the dimming corrected observations. The least square regression is

$$DM^* - 2.5 \log (1 + z) = 5.15 \log (r) + 43.37. \tag{22}$$

Since the standard deviation of the slope is 0.18, the slope is also statistically consistent with the theoretical slope of 5 for the flat static universe.

The least squares regression parameters for the SNs, BCGs and GRBs are listed in Table 2.

TABLE 2
Modified Hubble Diagram Parameters for SNs, GRBs and BCGs
Assuming the Static Universe Model

	#	Outliers	Slope	Constant	Std Dev
SNs Essence Survey (Dimming Corr)	60	1	5.00 (0.17)	43.53 (0.02)	0.16
SNs HST Riess (Dimming Corr)	41	1	5.16 (0.27)	43.54 (0.07)	0.25
GRBs Firmani (Dimming Corr)	19	1	5.15 (0.18)	43.37 (0.07)	0.25
BCGs Diff Observers (InterGal Abs Corr)	22				
Observed		1	5.05 (0.16)	21.78 (0.08)	0.34
Fund Plane Corr		0	5.01 (0.13)	21.73 (0.06)	0.27
BCGs Collins & Mann (InterGal Abs Corr)	47				
Aperture Corr		4	5.04 (0.18)	17.66 (0.14)	0.32

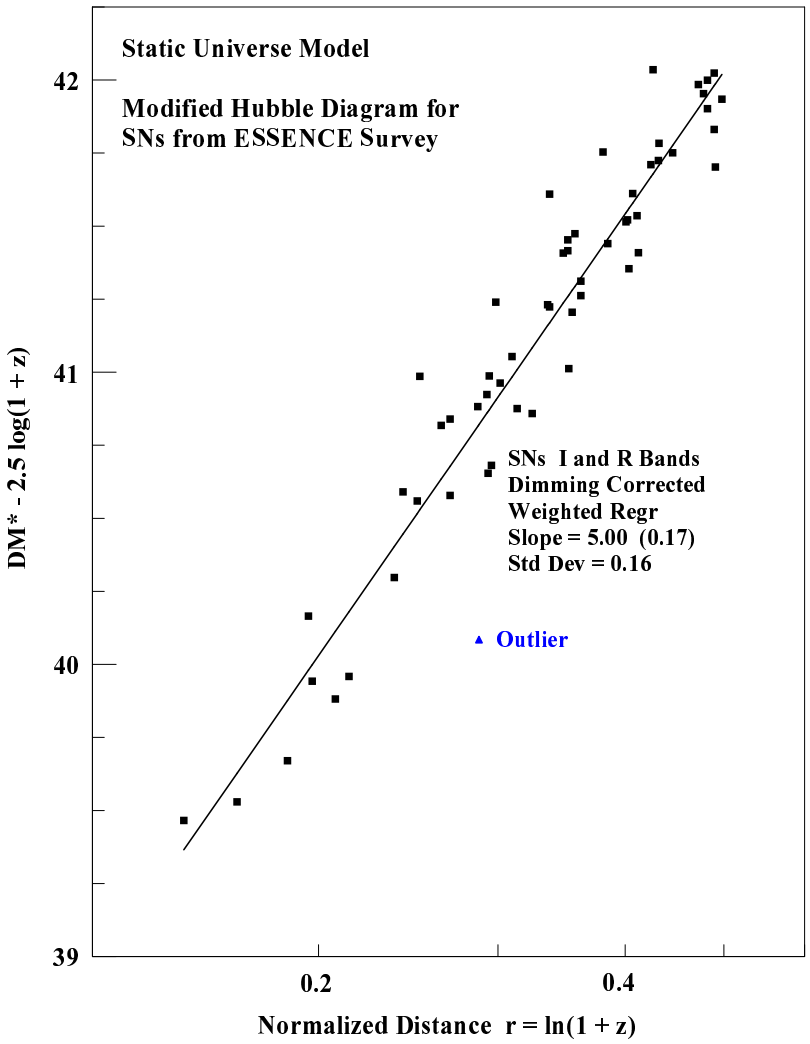

Figure 8: A modified Hubble diagram for SNs from the ESSENCE Survey is shown assuming the flat Static Universe model. The black squares represent the dimming corrected observations, DM*, less 2.5Log(1 + z). The blue diamonds represent the outliers. The black line is the least squares regression for the dimming corrected observations, DM*, less 2.5 log(1 + z).

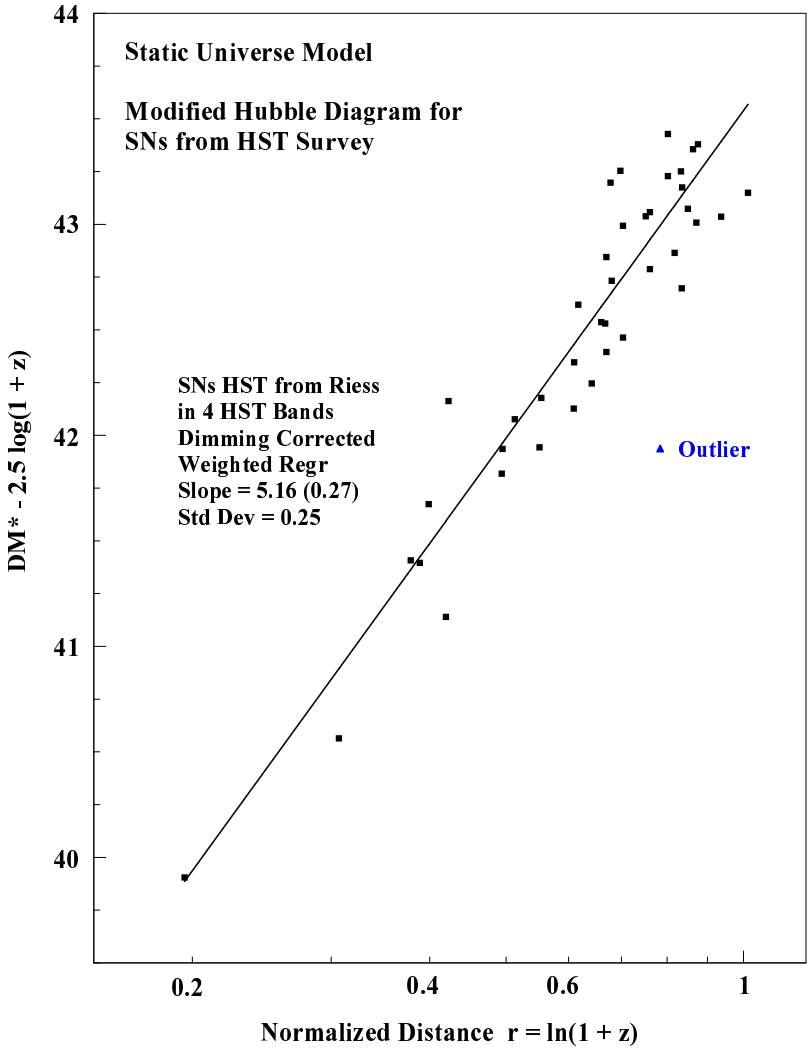

Figure 9: A modified Hubble diagram for SNs from the HST Survey is shown assuming the flat Static Universe model. The black squares represent the dimming corrected observations, DM*, less 2.5 log(1 + z). The blue diamonds represent the outliers. The black line is the least squares regression for the dimming corrected observations, DM*, less 2.5 log(1 + z).

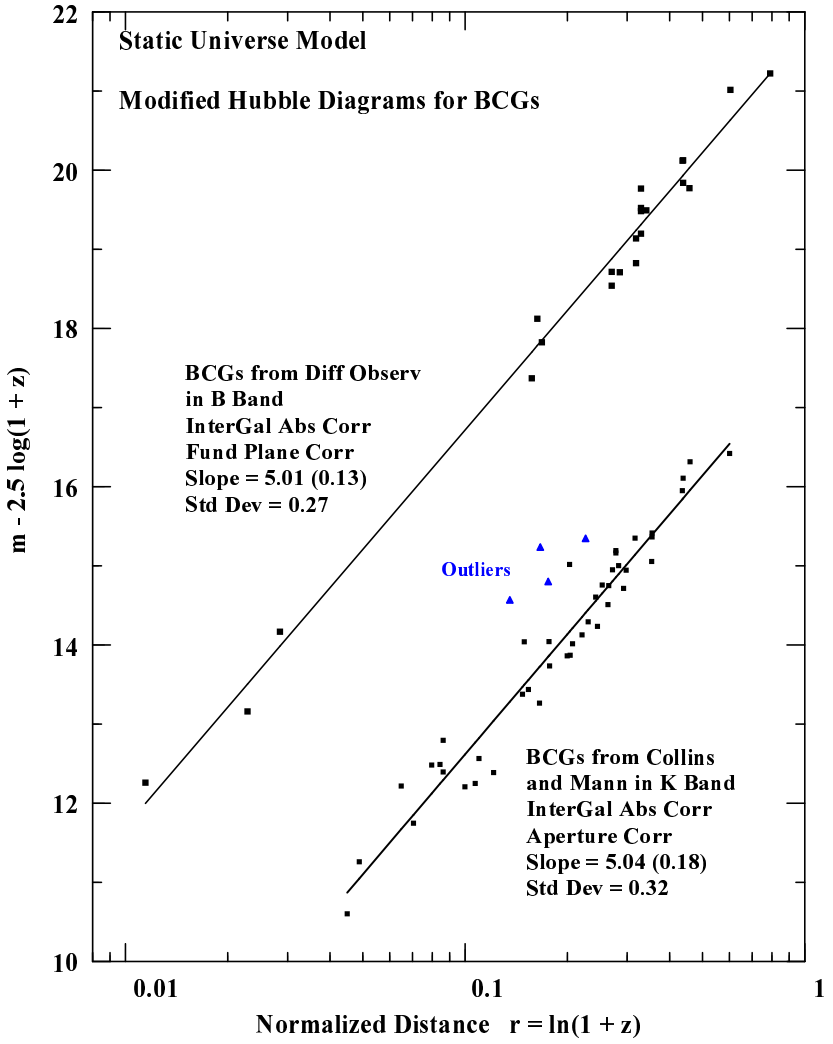

Figure 10: Modified Hubble diagrams for the BCGs are shown assuming the flat Static Universe model. The black squares represent the apparent magnitudes, m, less 2.5 log(1 + z). The blue diamonds represent the outliers. The black line is the least squares regression for the apparent magnitudes, m, less 2.5 log(1 + z).

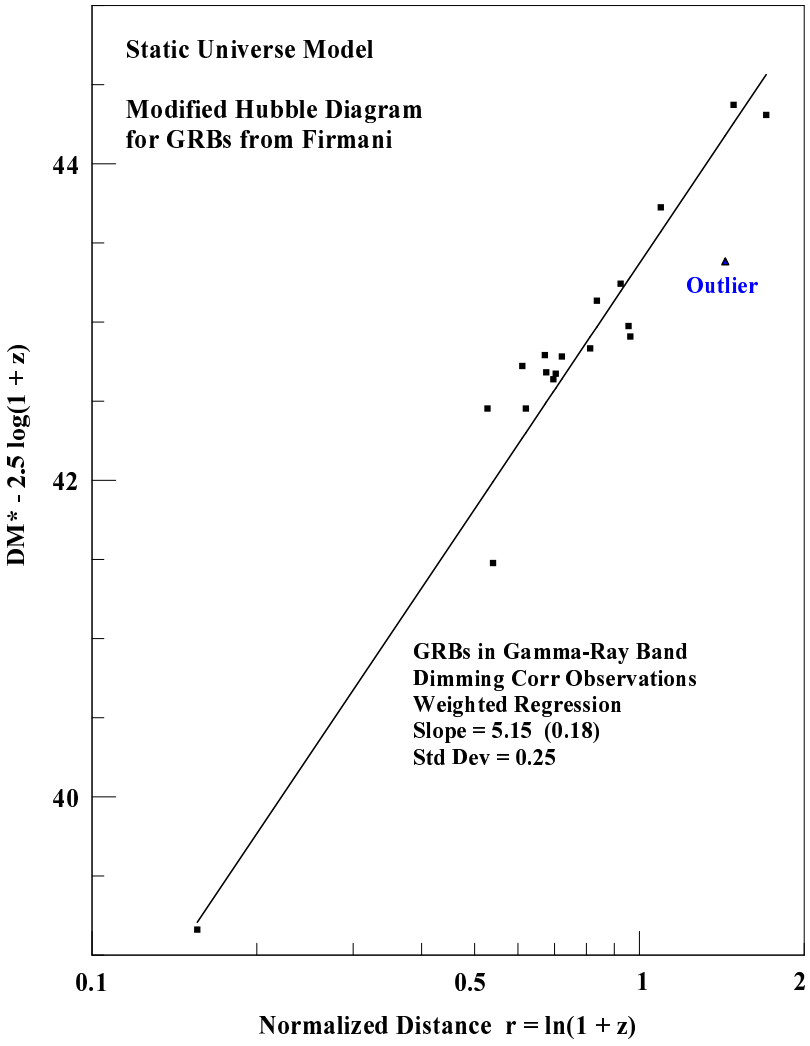

Figure 11: A modified Hubble diagram is shown for the GRBs assuming the flat Static Universe model. The black squares represent the dimming corrected observations, DM*, less 2.5 log(1 + z). The blue diamond is an outlier. The black line is the least squares fit to each of the dimming corrected observations, DM*, less 2.5 log(1 + z).

8 Non-Evolution of the Brightest Cluster Galaxies

The Hubble diagram of the BCGs from Different Observers is shown to closely fit the static universe model with a slope of 5.01. This is strong evidence that the BCGs do not evolve in luminosity.

However, it can also be logically proved that the BCGs do not evolve in luminosity. The argument depends on the non-evolution of SNs (discussed in Section 2) and the proof (in Section 5) showing that BCGs are not subject to anomalous dimming.

Consider the equation for the apparent magnitudes with terms for luminosity evolution, E(z), and anomalous dimming, D(z), which may depend on the redshift. For the static universe model, the equation for the apparent magnitude, m, is given by

$$m - 2.5 \log (1 + z) = M + E(z) + D(z) + 5 \log (r) + C. \tag{23}$$

Note that equation 23 without E(z) and D(z) is linear because the dependent variable, m, is replaced by m - 2.5 log(1 + z) as in equation 14.

Since the SNs in theory (and practice) do not evolve in luminosity, E(z) = 0 in equation 23. Furthermore, for SNs, D(z) = 2.5 log(1 + z). Therefore, by subtracting 2.5 log(1 + z) from both sides of the equation 23, the equation for SNs becomes

$$m^* - 2.5 \log (1 + z) = M + 5 \log (r) + C \tag{24}$$

where m* = m - 2.5 log(1 + z) is the dimming corrected apparent magnitude.

For BCGs, it is proved that anomalous dimming does not occur in Section 5. Consequently, in equation 23, D(z) = 0 for the BCGs. Then, the equation for the BCGs is given by

$$m - 2.5 \log (1 + z) = M + E(z) + 5 \log (r) + C. \tag{25}$$

But, Figure 10 clearly shows that the regression line slopes for the BCGs from Different Observers and the BCGs from Collins and Mann are nearly the same as the regression line slopes for the SNs in Figures 8 and 9 and the GRBs in Figure 11. This clearly requires E(z) = 0 in equation 25 for the BCGs and proves the BCGs do not evolve in luminosity.

8.1 Theoretical Basis for a Non-Evolving Universe

In the expanding universe model, it is assumed that the universe began a finite time ago in a singularity. Galaxies formed shortly after this time and the stars in the galaxies evolved to their present state as the universe expanded. Thus, evolution of galaxies must occur in the expanding universe model.

On the other hand, observations presented in this paper show that the universe is static and in a non-evolving state. In this state, although individual stars and galaxies change, the same mix of stars and galaxies, i.e., the same galaxy population as locally observed, is present at any redshift. Consequently, no evolutionary corrections have to be applied to galaxies and supernovae.

The concept of non-evolution follows directly from the perfect cosmological principle (PCP) which was proposed in 1948 by Bondi and Gold [21]. The PCP says the universe looks the same from any location at any time. Bondi and Gold based the reality of the PCP on the following paradigm:

> As the physical laws cannot be assumed independent of the structure of the universe and, conversely, the structure of the universe depends upon the physical laws, it follows that the universe is in a stable self-perpetuating state, without making any assumptions regarding the particular features which lead to this stability.

Bondi and Gold emphasized that only in such an equilibrium universe can the constants and laws of physics be invariant to both changes in location and time. Note: Bondi and Gold also assumed that the universe expands. However, I believe that given the strong arguments for the PCP, the PCP should hold in a static universe.

At the present time, the PCP must be considered an even stronger theoretical principle since the invariance of the physical constants [22] and the laws of physics are confirmed both by local experiments and by distant observations of the universe.

9 Tolman Surface Brightness Test

The theoretical relation between the average surface brightness, μ_e, and the Hubble redshift is given by

$$\mu_e = A\ [2.5 \log (1 + z)] + C \tag{26}$$

where A is the slope and C is a constant. In the static universe, the theoretical slope is 1. For the expanding universe model, the theoretical slope is 4. The importance of the surface brightness test is due to the fact that it is independent of the metric of the universe. Thus, it is a specific test for whether the universe is static or expanding. This is generally called the Tolman Surface Brightness Test since Tolman derived the relation for the expanding universe in 1930. Later, in 1972, it was realized by Geller and Peebles that the test would also apply to a static universe with only one factor of $1/(1 + z)$.

The surface brightness plot for the BCGs from Different Observers is shown in Fig. 12. The observed surface brightness is corrected for inter galactic dust absorption. The regression equation is given by

$$\mu_e = 1.02\ [2.5 \log (1 + z)] + 23.56. \tag{27}$$

The standard deviation for the slope is 0.36 magnitudes. Therefore, since the observed slope is statistically consistent with a slope of 1, this conclusively proves that the universe is static.

Note: Lerner [23] has also concluded from surface brightness observations of galaxies between z = 5 and z = 6 in the Hubble Ultra Deep Field that the universe is "non-expanding" (static).

10 Angular Size Test

The theoretical relation between the effective angular radius, θ and the normalized distance, r = ln(1 + z), in a flat static universe is given by

$$\theta = \frac{R_e}{29.09\ r}. \tag{28}$$

calculated assuming H = 50 Km/sec/Mpc.

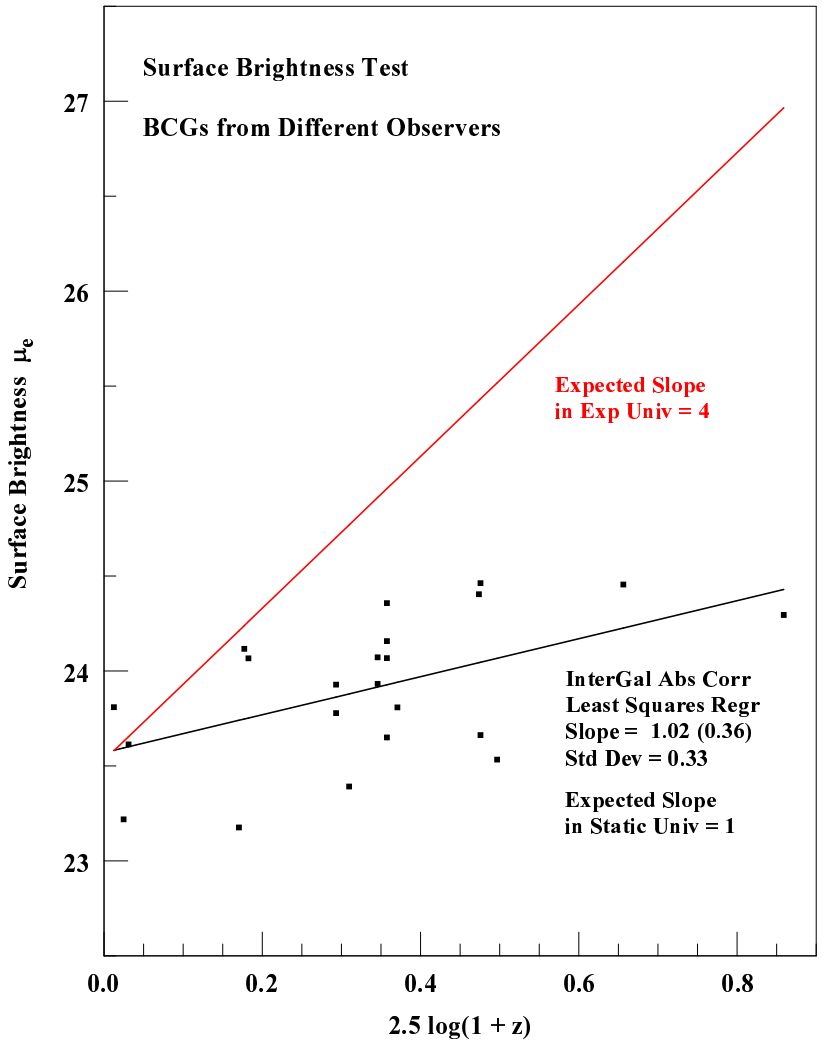

Figure 12: The Tolman surface brightness test of the BCGs from Different Observers is shown. The black squares represent the observations. The black line shows the least squares fit to the observed surface brightness. The red line represents the theoretical surface brightness expected in the expanding universe model.

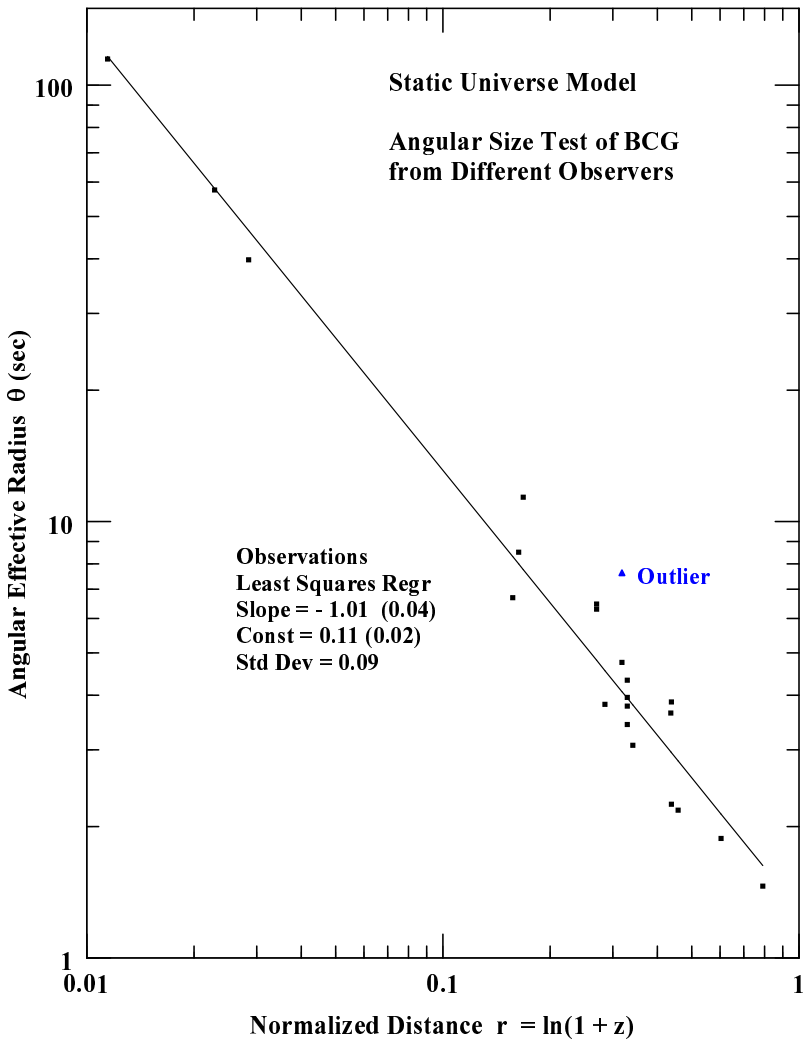

Figure 13: The Effective Angular Radii of the BCGs from Different Observers are plotted versus the normalized distance, r. The observations are shown as solid squares. The blue diamond is an outlier. The solid line is the least squares regression.

Taking logarithms of equation 28, the equation is changed to a

$$\log(\theta) = A\log(r) + C. \tag{29}$$

This is a linear equation with a slope A and constant C. Theoretically, the slope is -1 in a flat static universe.

The angular effective radii for the BCGs from Different Observers are plotted in Fig. 13 assuming a static universe. The least squares regression line is given by

$$\log(\theta) = -1.01\log(r) + 0.11. \tag{30}$$

Since the observed slope of -1.01 has a standard deviation of 0.04, the slope is statistically consistent with a slope of -1, thus indicating the universe is static.

11 Comments

The main results of this paper are the derivation of the anomalous dimming effect effect for the SNs and GRBs and the falsification of the expanding universe model. This lead to the conclusion that the universe is static. However, this conclusion introduces a new problem - determining the cause of the Hubble redshift in a static universe. This problem is addressed in Andrews [24] where the Hubble redshift is derived from a wave system theory of the universe.

Observations show that BCGs do not evolve in luminosity. This can only be true if the universe is in an equilibrium state, presumably, a state of maximum entropy. A corollary is that physical processes must exist which maintain the universe in an equilibrium state.

12 Acknowledgment

As is well known, the scientific method requires that new theories must be verified by (accurate) observational data. Therefore, I gratefully acknowledge the excellent work of the observers referenced in this paper.

References

[1] Shapiro, C.A., & Turner, M.S. (2005), What Do We Really Know About Cosmic Acceleration?, preprint (astro-ph/051258v1 23 Dec 2005).

[2] Collins, C.A., & Mann, R.G. (1998), The K-Band Hubble Diagram for Brightest Cluster Galaxies in X-Ray Clusters, MNRAS 297, 128.

[3] Sandage, A. (1972), The Redshift-Distance Relation. 1. Angular Diameter of First-Ranked Cluster Galaxies as a Function of Redshift: The Aperture Correction to Magnitudes, ApJ 173, 485.

[4] Wood-Vasey et al (2007), Observational Constraints on the Nature of the Dark Energy: First Cosmological Results for the ESSENCE Survey, preprint (astro-ph/0701041v1) 2 Jan 2007.

[5] Riess, A. et al (2006), New Hubble Space Telescope Discoveries of Type Ia Supernovae at z > 1: Narrowing Constraints on the Early Behavior of Dark Energy, preprint (astro-ph/0611572v2 20 Dec 2006).

[6] Riess, A. et al (2004), Type Ia Supernova Discoveries at z > 1 from the Hubble Space Telescope: Evidence for Past Decelleration and Constraints on Dark Energy Evolution, preprint (astro-ph/0402512v2 31 Mar 2004).

[7] Firmani, C. et al (2006) The Hubble diagram extended to z >> 1: the γ-Ray Properties of GRBs Confirm the ΛCDM Model, preprint (astro-ph/0605430v2 23 Sep 2006). Note: Version 2 of the paper appeared in MNRAS 28 February 2008.

[8] Firmani et al (2006) Discovery of a Tight Correlation Among the Prompt Emission Properties of Long GRBs, preprint (astro-ph/0605073v1 2 May 2006). Note: Version 1 of the paper appeared in MNRAS 28 February 2008.

[9] Avilla-Reese, V. et al (2008), Gamma-Ray Bursts, New Cosmological Beacons, preprint (astro-ph/0802.2578 22 Feb 2008).

[10] Menard, B. et al (2009), Measuring the Galaxy-Mass and Galaxy-Dust Correlations Through Magnification and Reddening, preprint (0902:4240v1v1[astro-ph.CO] 25 Feb 2009).

[11] Fukugita, M., Shimasaku, K., & Ichikawa, T. (1995), Galaxy Colors in Various Photometric Band Systems, PASP 107, 945.

[12] Aragon-Salamanca et al. (1993), Evidence for Systematic Evolution in the Properties of Galaxies in Distant Clusters, MNRAS 262, 764.

[13] Saglia, R.P. et al. (1993), The Effects of Seeing on the Photometric Properties of Elliptical Galaxies, MNRAS 264, 961.

[14] Towne, D.H. (1967), "Wave Phenomena", Addison-Wesley Publishing Company, pages 345-347.

[15] Kocher, C.A. (1988), Experiments with Fourier Transforms at Radio Frequencies, Am J Physics. 56, 524.

[16] Lieu, R., & Mittaz, J. (2003), The Phase Coherence of Light from Extragalactic Sources: Direct Evidence Against First Order Planck Scale Fluctuations in Time and Space, preprint (astro-ph/0308305 27 Jan 2007).

[17] Weinberg, S.W. ((1972), Gravitation and Cosmology: Principles and Applications of the General Theory of Relativity, John Wiley & Sons, Inc, Pages 29-30.

[18] Goldhaber, G. et al. (2001), Timescale Stretch Parameterization of Type Ia Supernova B-band Light Curves, preprint (astro-ph/0104382v1 24 Apr 2008).

[19] Blondin, S. et al (2008), Time Dilation in Type Ia Supernova Spectra at High Redshifts, preprint (astro-ph/0804:3595v1 22 Apr 2008).

[20] Sandage, A.R., Kron, R.G. & Longair, M.S. (1995), "The Deep Universe", Springer-Verlag, New York, page 78.

[21] Bondi, H., & Gold, T. (1948), The Steady-State Theory of the Expanding Universe, MNRAS 108, 252.

[22] Varshalovich, D.A., Potekhin, A.Y., & Ivanchik, A.V. (2000), Testing Cosmological Variability of the Fundamental Constants, preprint (physics/0004062v1 25 Apr 2000).

[23] Lerner, E.J. (2006), Evidence for a Non-Expanding Universe: Surface Brightness Data from HUDF, "1st Crisis in Cosmology Conference, CCC-1", AIP Conference Proceedings, 822, 60.

[24] Andrews, T.B. (2006), Derivation of the Hubble Redshift and the Metric in a Static Universe, "1st Crisis in Cosmology Conference, CCC-1", AIP Conference Proceedings, 822, 123.

Note: The following references refer to the observer groups responsible for observation of the BCGs from Different Observers.

[25] Jorgensen, I., Franx, M., & Kjaergaard, P. (1995), Multicolour CCD Surface Photometry for E and SO Galaxies in 10 Clusters, MNRAS 273, 1097.

[26] Barger, A.J. et al. (1998), New Constraints on the Luminosity Evolution of Spheroidal Galaxies in Distant Clusters, ApJ 501, 522.

[27] Jorgensen, I., Franx. M., & Kjaergaard, P. (1999), The Evolution of Cluster E and SO Galaxies Measured from the Fundamental Plane, preprint (astro-ph/9905155v1 13 May 1999).

[28] Kelson, D.D. et al. (1999), The Evolution of Early-Type Galaxies in Distant Clusters I: Surface Photometry and Structural Parameters for 53 Galaxies in the z = 0.33 Cluster CL1358+62, Preprint (astro-ph/9911065v1 4 Nov 1999).

[29] Bender, R. et al. (1998), Exploring Cluster Elliptical Galaxies as Cosmological Standard Rods, ApJ 493, 529.

[30] van Dokkum, P.G. & Franx, Marijn (1996), The Fundamental Plane in CL0024 at $z = 0.4$: Implications for the Evolution of the Mass-to-Light Ratio, MNRAS 281, 985.

[31] Dickinson, M. (1996), Cluster Ellipticals at High redshift: The View from the Ground and with HST, "Fresh Views of Elliptical Galaxies," ed. Buzzoni, A., Renzini, A., & Serrano, A., ASP Conference Series, Vol. 86, 283.

[32] Ziegler, B.L. et al. (1999), Probing Early-Type Galaxy Evolution with the Kormendy Relation, Preprint (astro-ph/9903222v1 15 Mar 1999).

[33] Kelson, D.D. et al. (1997), Evolution of Early-Type Galaxies in Distant Clusters: The Fundamental Plane from Hubble Space Telescope Imaging and Keck Spectroscopy, ApJ 478, L13.

[34] van Dokkum, P.G. et al. (1998), Luminosity Evolution of Early-Type Galaxies to z = 0.83: Constraints on Formation Epoch and Omega, ApJ 504, L17.

Note: All preprints refer to the http://arXiv.org/ website

A Appendix: Observations and Calculated Parameters

Table A1 lists the observations and calculated parameters for Type Ia Supernovae (SNs) ordered by redshift from the ESSENCE Survey. The basic observations are the redshift, z, the distance modulus, DM, the standard deviation of the distance modulus. The calculated values are r, the normalized distance in the static universe, DM*, the dimming corrected distance modulus observations and the least squares regression for DM*.

Table A2 lists the observations and calculated parameters for Type Ia Supernovae (SNs) ordered by redshift from the HST Riess Survey. The parameters are the same as listed in Table 1.

Tables A3 and A4 list the observations and calculated parameters ordered by redshift for the Brightest Cluster Galaxies (BCGs) from Different Observers. The basic observations are the velocity dispersion, redshift, z, the observed average surface brightness, μ, and the observed effective angular radius, θ. μ(B) is shown corrected to the B band and corrected for inter-Galactic dust absorption. Also listed in Table 4 are the corrected apparent magnitudes, the effective radii of the BCG in Kpc, assuming H_o = 50 Km/sec/Mpc and, finally, the apparent magnitudes and absolute magnitudes corrected using the Fundamental Plane method.

Tables A5 and A6 list the observations and calculated parameters ordered by redshift for the BCGs from Collins and Mann. The basic observations and corrections are in Table 5. These include the redshift, z, the apparent magnitude, m(K), measured within a 25 Kpc radius aperture calculated assuming the Friedman expanding universe model with $q_0 = 0.5$ and H_o = 50 Km/sec/Mpc, the intergalactic Abs, K-corrections and seeing corrections. Table 6 lists the calculations required to estimate the aperture corrections from the expanding universe model to the static universe model. The aperture corrected apparent magnitudes, m(K) and the absolute magnitudes, M(K), are listed in the last two columns. The aperture corrected m(K) is represented by the red line in Figure 3.

Table A7 lists the observations and calculated parameters ordered by redshift of the GRBs from Firmani. The basic observations are the redshift, z, the distance modulus, DM, and the estimated standard deviations of the DM values. In the last two columns, the dimming corrected observations, DM*, and the static least squares regression of DM* are listed.

Table A8 lists the observations from Goldhaber ordered by redshift. The basic observations are the redshift the light curve broadening factor, w, and the standard deviation of the width factor. The least square weighted regression for w, assuming w is zero at zero redshift, is listed in the last column.

TABLE A1
Type Ia Supernovae from ESSENCE SURVEY
Observations and Calculated Parameters

SNs	z	r	DM	Std Dev	DM*	Regr DM*
	Data	Calc	Data	Data	Dimm Corr	Dimm Corr
		Static				Static
e020	0.159	0.148	39.786	0.268	39.63	39.53
k429	0.181	0.166	39.891	0.138	39.71	39.81
d086	0.205	0.186	40.075	0.284	39.87	40.08
n404	0.216	0.196	40.590	0.290	40.38	40.20
g005	0.218	0.197	40.371	0.242	40.16	40.22
h363	0.231	0.208	40.333	0.319	40.11	40.34
e132	0.239	0.214	40.424	0.275	40.19	40.42
n326	0.268	0.237	40.813	0.244	40.56	40.66
k425	0.274	0.242	41.116	0.257	40.85	40.71
p455	0.284	0.250	41.102	0.269	40.83	40.79
m027	0.286	0.252	41.532	0.306	41.26	40.80
g055	0.302	0.264	41.391	0.353	41.10	40.92
n278	0.309	0.269	41.163	0.190	40.87	40.97
d117	0.309	0.269	41.424	0.255	41.13	40.97
e029	0.332	0.287	41.505	0.260	41.19	41.13
d083#	0.333	0.287	40.709	0.104	40.40	41.13
g097	0.340	0.293	41.559	0.292	41.24	41.18
m193	0.341	0.293	41.291	0.212	40.97	41.18
d149	0.342	0.294	41.626	0.182	41.31	41.19
h364	0.344	0.296	41.323	0.143	41.00	41.20
h359	0.348	0.299	41.888	0.255	41.56	41.23
e136	0.352	0.302	41.618	0.251	41.29	41.25
d093	0.363	0.310	41.726	0.101	41.39	41.32
n263	0.368	0.313	41.556	0.139	41.22	41.35
g052	0.383	0.324	41.563	0.199	41.21	41.43
g142	0.399	0.336	41.960	0.420	41.60	41.52
d085	0.401	0.337	41.956	0.199	41.98	41.53
k448	0.401	0.337	42.342	0.388	41.59	41.53
k485	0.416	0.348	42.163	0.386	41.79	41.61
h342	0.421	0.351	42.179	0.120	41.80	41.64
g133	0.421	0.351	42.216	0.314	41.83	41.64
f235	0.422	0.352	41.777	0.213	41.39	41.64
b013	0.426	0.355	41.976	0.205	41.59	41.66
e148	0.429	0.357	42.249	0.178	41.86	41.68
d089	0.436	0.362	42.048	0.168	41.66	41.71
d097	0.436	0.362	42.097	0.143	41.70	41.71
m158	0.463	0.380	42.580	0.260	42.17	41.84
e108	0.469	0.385	42.275	0.125	41.86	41.87
g160	0.493	0.401	42.385	0.240	41.95	41.98
h319	0.495	0.402	42.395	0.180	41.96	41.99
e149	0.497	0.403	42.230	0.243	41.79	42.00
h283	0.502	0.407	42.495	0.353	42.05	42.02
p524	0.508	0.411	42.428	0.195	41.98	42.04
g120	0.510	0.412	42.304	0.187	41.86	42.05
n285	0.528	0.424	42.631	0.243	42.17	42.13
d033	0.531	0.426	42.960	0.138	42.50	42.14
f011	0.539	0.431	42.661	0.224	42.19	42.17

Continued next page

TABLE A1
Type Ia Supernovae from ESSENCE Survey (Continued)
Observations and Calculated Parameters

SNs	z Data	r Calc Static	DM Data	Std Dev Data	DM* Dimm Corr	Regr DM* Dimm Corr Static
f244	0.540	0.432	42.721	0.240	42.25	42.17
f041	0.561	0.445	42.718	0.135	42.23	42.26
h323	0.603	0.472	43.009	0.201	42.50	42.41
e138	0.612	0.477	42.990	0.155	42.47	42.44
d084	0.619	0.482	42.948	0.274	42.42	42.47
f231	0.619	0.482	43.046	0.142	42.52	42.47
e140	0.631	0.489	42.893	0.150	42.55	42.51
n256	0.631	0.489	43.086	0.108	42.36	42.51
g050	0.633	0.490	42.767	0.150	42.23	42.51
e147	0.645	0.498	43.015	0.155	42.47	42.55
h300	0.687	0.523	43.092	0.142	42.52	42.69
g240	0.687	0.523	43.038	0.177	42.47	42.69
p454	0.695	0.528	43.530	0.137	42.96	42.71

Outliers

TABLE A2
Type Ia Supernovae from HST (Riess) Survey
Observations and Calculated Parameters

SNs	Sample	z Data	r Calc Static	DM Data	Std Dev Data	DM* Dimm Corr	Regr DM* Dimm Corr Static
2002kc	Silver	0.216	0.196	40.33	0.19	40.12	39.89
HST04Kur	Silver	0.359	0.307	41.23	0.39	40.90	40.89
HST04Yow	Gold	0.460	0.378	42.23	0.32	41.82	41.36
2002dc	Gold	0.475	0.389	42.24	0.20	41.82	41.42
HST04Hawk	Silver	0.490	0.399	42.54	0.24	42.11	41.48
HST05Zwi	Silver	0.521	0.419	42.05	0.37	41.59	41.60
2002hr	Silver	0.526	0.423	43.08	0.27	42.62	41.82
HST05Dic	Silver	0.638	0.493	42.89	0.18	42.35	42.29
2003be	Gold	0.640	0.495	43.01	0.25	42.47	42.37
2003bd	Gold	0.670	0.513	43.19	0.34	42.63	42.47
2002kd	Gold	0.735	0.551	43.14	0.19	42.54	42.64
HST04Rak	Gold	0.740	0.554	43.38	0.22	42.78	42.67
HST05Spo	Gold	0.839	0.609	43.45	0.20	42.79	42.89
2003eq	Gold	0.840	0.610	43.67	0.21	43.01	42.97
HST04Man	Gold	0.854	0.617	43.96	0.29	43.29	43.00
2003eb	Gold	0.900	0.642	43.64	0.25	42.94	43.10
2003XX	Gold	0.935	0.660	43.97	0.29	43.25	43.21
2002dd	Gold	0.950	0.668	43.98	0.34	43.25	43.24
HST04Tha	Gold	0.954	0.670	43.85	0.27	43.12	43.30
2003es	Gold	0.954	0.670	44.30	0.27	43.57	43.30
HST04Pat	Gold	0.970	0.678	44.67	0.36	43.93	43.34
HST04Omb	Gold	0.975	0.681	44.21	0.26	43.47	43.37
HST05Str	Gold	1.010	0.698	44.77	0.19	44.01	43.45
HST05Fer	Gold	1.020	0.703	43.99	0.27	43.23	43.48
HST04Eag	Gold	1.020	0.703	44.52	0.19	43.76	43.48
HST05Gab	Gold	1.120	0.751	44.67	0.18	43.85	43.63
2002ki	Gold	1.140	0.761	44.71	0.29	43.88	43.66
HST04Gre	Gold	1.140	0.761	44.44	0.31	43.61	43.67
HST05Red#	Silver	1.190	0.784	43.64	0.39	42.79	43.75
HST05Lan	Gold	1.230	0.802	44.97	0.20	44.10	43.81
HST05Koe	Gold	1.230	0.802	45.17	0.23	44.30	43.81
2003az	Silver	1.265	0.818	44.64	0.25	43.75	43.90
2002fw	Gold	1.300	0.833	45.06	0.20	44.16	43.96
2002hp	Gold	1.305	0.835	44.51	0.30	43.60	43.96
2003aj	Silver	1.307	0.836	44.99	0.31	44.08	43.99
2003dy	Gold	1.340	0.850	44.92	0.31	44.00	44.05
HST04Mcg	Gold	1.370	0.863	45.23	0.25	44.29	44.08
HST04Sas	Gold	1.390	0.871	44.90	0.19	43.95	44.12
2002fx	Silver	1.400	0.875	45.28	0.81	44.33	44.15
2003ak	Silver	1.551	0.936	45.07	0.32	44.05	44.30
1997ff	Gold	1.755	1.013	45.35	0.35	44.25	44.48

Outliers

TABLE A3
Brightest Cluster Galaxies from Different Observers
Observations

BCG	Ref	Vel Disp Km/sec	z Data	r Calc Static	μ_e Data	Filter Band	Conv to B	μ_e Filter Corr
HydraI N3311	[25]	196	0.0115	0.0114	22.58	Gunn r	1.23	23.81
Coma D129	[25]	254	0.0231	0.0229	23.22	B		23.22
A539 D47	[25]		0.0289	0.0285	22.38	Gunn r	1.23	23.61
A2218	[26]		0.1700	0.1570	23.18	B		23.18
A2218-L244	[27]	209	0.1772	0.1631	23.16	V_z	0.96	24.12
A665-1150	[27]	298	0.1831	0.1681	23.11	V_z	0.96	24.07
3 Clust[1]	[26]		0.3100	0.2700	23.79	B		23.79
3 Clust[1]	[26]		0.3100	0.2700	23.94	B		23.94
CL1358+62 375	[28]	308	0.3300	0.2852	22.44	V_z	0.96	23.40
MS1512+36 9	[29]	294	0.3750	0.3185	23.95	B		23.95
A370 20#	[29]	342	0.3750	0.3185	24.09	B		24.09
3 Clust[2]	[26]		0.3900	0.3293	24.18	B		24.18
3 Clust[2]	[26]		0.3900	0.3293	24.38	B		24.38
3 Clust[2]	[26]		0.3900	0.3293	24.09	B		24.09
CL0024+16 161	[30]	393	0.3900	0.3293	22.70	V_z	0.96	23.66
Abell 851	[31]		0.4070	0.3415	23.83	B		23.83
CL0016 139	[32]		0.5470	0.4363	24.44	B		24.44
3 Clust[3]	[26]		0.5500	0.4383	24.50	B		24.50
3 Clust[3]	[26]		0.5500	0.4383	23.70	B		23.70
MS2053-04 197	[33]	328	0.5800	0.4574	22.60	V_z	0.96	23.56
MS1054-03 1484	[34]	342	0.8300	0.6043	24.50	B_z		24.50
3C324	[31]		1.2060	0.7912	24.44	B		24.44

(1) AC103, AC104 and AC118
(2)CL1447+23, CL0024+16 and CL0054-27
(3) CL1601-42 and CL0016+16
Outlier

TABLE A4
Brightest Cluster Galaxies from Different Observers
Calculated Parameters

BCG	InterGal Dust Abs	μ_e(B) InterGal Abs Corr	θ Data	m_e(B) InterGal Abs Corr	R_e Calc Static	m_e(B) Fund Plane Corr	M_e(B) Fund Plane Corr
HydraI N3311	0.00	23.81	114.82	12.27	38.22	12.27	-21.92
Coma D129	0.00	23.22	57.54	13.18	38.26	13.18	-22.53
A539 D47	0.00	23.61	39.81	14.37	32.99	14.20	-22.00
A2218	0.01	23.18	6.69	17.80	30.55	17.54	-22.50
A2218-L244	0.00	24.12	8.51	18.22	40.39	18.30	-21.83
A665-1150	0.00	24.07	11.38	17.54	55.64	18.01	-22.19
3 Clust[1]	0.02	23.78	6.47	18.48	50.82	18.83	-22.51
3 Clust[1]	0.02	23.93	6.30	18.69	49.49	19.01	-22.33
CL1358+62 375	0.01	23.39	3.81	19.24	31.63	19.02	-22.46
MS1512+36 9	0.02	23.93	4.76	19.31	44.05	19.48	-22.27
A370 20#	0.02	24.07	7.63	18.42	70.72	19.17	-22.58
3 Clust[2]	0.02	24.16	4.33	19.74	41.48	19.84	-22.00
3 Clust[2]	0.02	24.36	3.95	20.13	37.87	20.13	-21.71
3 Clust[2]	0.02	24.07	3.78	19.94	36.16	19.88	-21.96
CL0024+16 161	0.01	23.65	3.43	19.73	32.84	19.55	-22.28
Abell 851	0.02	23.81	3.07	20.13	30.49	19.86	-22.07
CL0016 139	0.04	24.40	3.64	20.37	46.20	20.59	-21.97
3 Clust[3]	0.04	24.46	3.86	20.30	49.21	20.60	-21.97
3 Clust[3]	0.04	23.66	2.25	20.67	28.68	20.32	-22.26
MS2053-04 197	0.02	23.53	2.18	20.59	29.03	20.27	-22.42
MS1054-03 1484	0.04	24.46	1.88	21.84	33.04	21.67	-21.78
3C324	0.14	24.29	1.46	22.30	33.60	22.08	-22.16

Outlier

TABLE A5
Brightest Cluster Galaxies from Collins and Mann Observations

Cluster	z	r Calc Static	m(K) Data Exp	InterGal Abs	K-Corr	Seeing Corr	m(K) Corr Exp
MS2354.4-3502	0.046	0.045	10.49	0.00	-0.12	0.00	10.61
MS0007.2-3532	0.050	0.049	11.14	0.00	-0.13	0.00	11.27
MS1531.2+3118	0.067	0.065	12.07	0.00	-0.16	0.00	12.23
MS0904.5+1651	0.073	0.070	11.59	0.00	-0.17	0.00	11.76
MS0301.7+1516	0.083	0.080	12.33	0.00	-0.17	0.00	12.50
MS1558.5+3321	0.088	0.084	12.33	0.00	-0.18	0.00	12.51
MS2216.0-0401	0.090	0.086	12.23	0.00	-0.18	0.00	12.41
MS2215.7-0404	0.090	0.086	12.63	0.00	-0.18	0.00	12.81
MS1127.7-1418	0.105	0.100	12.02	0.00	-0.21	0.00	12.23
MS2124.7-2206	0.113	0.107	12.05	0.00	-0.22	0.00	12.27
MS1522.0+3003	0.116	0.110	12.36	0.00	-0.23	0.00	12.59
MS1111.8-3754	0.129	0.121	12.16	0.00	-0.25	0.00	12.41
MS0955.7-2635#	0.145	0.135	14.32	0.00	-0.28	-0.00	14.60
MS0433.9+0957	0.159	0.148	13.11	0.00	-0.31	-0.01	13.41
MS1618.9+2552	0.161	0.149	13.77	0.00	-0.31	-0.01	14.07
MS1004.2+1238	0.166	0.154	13.16	0.00	-0.32	-0.01	13.47
MS0906.5+1110	0.180	0.166	12.97	0.00	-0.34	-0.01	13.30
MS1125.3+4324	0.181	0.166	14.94	0.00	-0.35	-0.01	15.27
MS0849.7-0521	0.192	0.176	14.49	0.00	-0.37	-0.01	14.84
R843053	0.193	0.176	13.73	0.00	-0.37	-0.01	14.08
MS0839.8+2938	0.194	0.177	13.42	0.00	-0.37	-0.01	13.77
MS1006.0+1202	0.221	0.200	13.52	0.00	-0.41	-0.02	13.90
MS0419.0-3848	0.225	0.203	14.67	0.00	-0.42	-0.02	15.06
MS1546.8+1132	0.226	0.204	13.52	0.00	-0.42	-0.02	13.91
MS1253.9+0456	0.230	0.207	13.66	0.00	-0.42	-0.02	14.06
MS2301.3+1506	0.247	0.221	13.75	0.01	-0.45	-0.02	14.18
MS0537.1-2834#	0.254	0.226	14.97	0.01	-0.46	-0.02	15.40
MS1455.0+2232	0.259	0.230	13.91	0.01	-0.46	-0.02	14.34
MS1617.1+3237#	0.274	0.242	14.22	0.01	-0.47	-0.03	14.66
R84155#	0.278	0.245	13.85	0.01	-0.47	-0.03	14.29
MS2255.7+2039	0.288	0.253	14.37	0.01	-0.48	-0.03	14.81
MS1008.1-1224	0.301	0.263	14.12	0.01	-0.49	-0.03	14.57
MS1147.3+1103	0.303	0.265	14.36	0.01	-0.49	-0.03	14.81
MS1241.5+1710	0.312	0.272	14.56	0.01	-0.49	-0.03	15.01
MS1426.4+0158	0.320	0.278	14.77	0.01	-0.50	-0.03	15.23
MS1532.5+0130	0.320	0.278	14.80	0.01	-0.50	-0.03	15.26
MS1224.7+2007	0.327	0.283	14.61	0.01	-0.50	-0.03	15.07
MS1208.7+3928	0.340	0.293	14.32	0.01	-0.51	-0.03	14.78
MS0821.5+0337	0.347	0.298	14.55	0.01	-0.51	-0.04	15.02
MS1512.4+3647	0.372	0.316	14.95	0.01	-0.53	-0.04	15.43
MS0302.5+1717	0.425	0.354	14.65	0.01	-0.55	-0.04	15.14
MS1621.5+2640	0.426	0.355	14.96	0.01	-0.55	-0.04	15.45
MS0302.7+1658	0.426	0.355	15.01	0.01	-0.55	-0.04	15.50
MS0015.9+1609	0.546	0.436	15.58	0.02	-0.56	-0.05	16.07
MS0451.6-0305	0.550	0.438	15.74	0.02	-0.56	-0.05	16.23
MS2053.7-0449	0.583	0.459	15.96	0.02	-0.56	-0.05	16.45
MS1054.4-0321	0.823	0.600	16.14	0.04	-0.57	-0.06	16.61

Outliers

TABLE A6
Brightest Cluster Galaxies from Collins and Mann
Calculated Parameters

Cluster	θ 25 Kpc Exp	R Calc Static	θ 25 Kpc Static	Δm Apert Corr	m(K) Apert Corr	M(K) Apert Corr
MS2354.4-3502	20.21	26.45	19.11	0.04	10.65	-26.55
MS0007.2-3532	18.72	26.57	17.61	0.04	11.31	-26.07
MS1531.2+3118	14.37	27.11	13.25	0.06	12.29	-25.73
MS0904.5+1651	13.32	27.30	12.20	0.06	11.82	-26.38
MS0301.7+1516	11.91	27.62	10.78	0.07	12.57	-25.92
MS1558.5+3321	11.32	27.78	10.19	0.08	12.58	-26.03
MS2216.0-0401	11.11	27.84	9.97	0.08	12.49	-26.17
MS2215.7-0404	11.11	27.84	9.97	0.08	12.89	-25.77
MS1127.7-1418	9.75	28.32	8.61	0.09	12.32	-26.68
MS2124.7-2206	9.18	28.58	8.03	0.10	12.37	-26.79
MS1522.0+3003	8.98	28.67	7.83	0.10	12.68	-26.53
MS1111.8-3754	8.24	29.09	7.08	0.11	12.52	-26.92
MS0955.7-2635#	7.52	29.60	6.35	0.12	14.72	-24.98
MS0433.9+0957	7.00	30.06	5.82	0.13	13.54	-26.36
MS1618.9+2552	6.94	30.12	5.76	0.13	14.20	-25.72
MS1004.2+1238	6.78	30.28	5.60	0.14	13.60	-26.38
MS0906.5+1110	6.38	30.74	5.19	0.15	13.45	-26.72
MS1125.3+4324	6.36	30.77	5.17	0.15	15.42	-24.76
MS0849.7-0521	6.09	31.13	4.89	0.15	14.99	-25.31
R843053	6.07	31.16	4.87	0.15	14.24	-26.08
MS0839.8+2938	6.05	31.19	4.85	0.16	13.93	-26.40
MS1006.0+1202	5.52	32.07	4.30	0.17	14.08	-26.53
MS0419.0-3848	5.46	32.21	4.23	0.18	15.24	-25.41
MS1546.8+1132	5.44	32.24	4.22	0.18	14.09	-26.57
MS1253.9+0456	5.38	32.37	4.15	0.18	14.24	-26.46
MS2301.3+1506	5.13	32.93	3.89	0.19	14.37	-26.48
MS0537.1-2834#	5.04	33.16	3.80	0.20	15.59	-25.32
MS1455.0+2232	4.97	33.32	3.73	0.20	14.54	-26.41
MS1617.1+3237*#	4.80	33.82	3.55	0.21	14.87	-26.20
R84155#	4.76	33.95	3.50	0.21	14.50	-26.60
MS2255.7+2039	4.66	34.28	3.40	0.22	15.03	-26.15
MS1008.1-1224	4.53	34.71	3.27	0.23	14.80	-26.48
MS1147.3+1103	4.52	34.78	3.25	0.23	15.04	-26.25
MS1241.5+1710	4.44	35.08	3.16	0.23	15.25	-26.11
MS1426.4+0158	4.38	35.34	3.10	0.24	15.46	-25.95
MS1532.5+0130	4.38	35.34	3.10	0.24	15.49	-25.92
MS1224.7+2007	4.32	35.58	3.04	0.24	15.31	-26.15
MS1208.7+3928	4.23	36.01	2.94	0.25	15.03	-26.51
MS0821.5+0337	4.18	36.25	2.89	0.25	15.27	-26.31
MS1512.4+3647	4.03	37.08	2.72	0.27	15.69	-26.04
MS0302.5+1717	3.77	38.87	2.43	0.29	15.44	-26.58
MS1621.5+2640	3.77	38.91	2.42	0.30	15.75	-26.28
MS0302.7+1658	3.77	38.91	2.42	0.30	15.80	-26.23
MS0015.9+1609	3.39	43.01	1.97	0.35	16.42	-26.14
MS0451.6-0305	3.38	43.15	1.96	0.35	16.58	-25.99
MS2053.7-0449	3.31	44.29	1.87	0.37	16.81	-25.89
MS1054.4-0321	3.02	52.76	1.43	0.46	17.07	-26.36

Outliers

TABLE A7
Gamma-Ray Bursts from Firmani
Observations and Calculated Parameters

GRB	z Data	r Calc Static	DM Data	Std Dev Data	DM* Dimm Corr	Regr DM* Dimm Corr Static
030329	0.1685	0.1557	39.50	0.23	39.33	39.43
970228	0.6950	0.5277	43.60	0.85	43.03	42.54
041006	0.7160	0.5400	42.65	0.50	42.06	42.60
990705	0.8424	0.6111	44.05	0.35	43.39	42.96
040924	0.8590	0.6200	43.80	0.50	43.13	43.00
970828	0.9578	0.6718	44.25	0.55	43.52	43.23
980703	0.9660	0.6760	44.15	0.47	43.42	43.25
021211	1.0060	0.6961	44.15	0.50	43.39	43.34
991216	1.0200	0.7031	44.20	0.56	43.44	43.37
000911	1.0580	0.7217	44.35	0.43	43.57	43.45
020813	1.2550	0.8131	44.60	0.42	43.72	43.81
990506	1.3070	0.8359	44.95	0.50	44.04	43.90
030328	1.5200	0.9243	45.25	0.32	44.25	44.21
990123	1.6000	0.9555	45.05	0.47	44.01	44.32
990510	1.6190	0.9628	45.00	0.30	43.95	44.35
030226	1.9860	1.0939	46.10	0.55	44.91	44.77
020124#	3.2000	1.4351	46.50	0.66	44.94	45.75
971214	3.4200	1.4861	47.60	0.38	45.99	45.88
000131	4.5000	1.7047	48.01	0.60	46.16	46.42

Outlier

TABLE A8
Observed Widths of Type Ia Supernovae
Light Curves from Goldhaber

SNs	z	(1 + z)	w	σ(w)	Regr w
	Data	Calc	Data	Data	
1992al	0.014	1.014	0.99	0.02	0.99
1992bo	0.018	1.018	0.77	0.01	1.00
1992bc	0.020	1.020	1.12	0.01	1.00
1992P	0.026	1.026	1.15	0.08	1.01
1992ag	0.026	1.026	1.14	0.04	1.01
1990O	0.030	1.030	1.09	0.03	1.01
1992bg	0.036	1.036	1.09	0.05	1.02
1992bl	0.043	1.043	0.92	0.03	1.02
1992bh	0.045	1.045	1.15	0.05	1.02
1990af	0.050	1.050	0.82	0.02	1.03
1993ag	0.050	1.050	1.01	0.04	1.03
1993O	0.052	1.052	0.99	0.01	1.03
1992bs	0.063	1.063	1.05	0.05	1.04
1993Bs	0.071	1.071	1.06	0.09	1.05
1992ae	0.075	1.075	1.09	0.09	1.05
1992bp	0.079	1.079	1.03	0.03	1.06
1992br#	0.088	1.088	0.58	0.04	1.07
1992aq	0.101	1.101	1.04	0.14	1.08
1997ac	0.320	1.320	1.39	0.03	1.29
1994F	0.354	1.354	0.96	0.19	1.33
1994am	0.372	1.372	1.22	0.05	1.34
1994H	0.374	1.374	1.19	0.07	1.35
1994an	0.378	1.378	1.44	0.23	1.35
1995ba	0.388	1.388	1.36	0.06	1.36
1995aw	0.400	1.400	1.62	0.06	1.37
1997am	0.416	1.416	1.55	0.07	1.39
1994al	0.420	1.420	1.22	0.13	1.39
1997Q	0.430	1.430	1.36	0.04	1.40
1996cn	0.430	1.430	1.28	0.10	1.40
1995az	0.450	1.450	1.41	0.10	1.42
1996cm	0.450	1.450	1.33	0.09	1.42
1997ai	0.450	1.450	1.52	0.20	1.42
1995aq	0.453	1.453	1.27	0.15	1.42
1992bi#	0.458	1.458	2.26	0.34	1.43
1995ar	0.465	1.465	1.42	0.21	1.44
1997P	0.472	1.472	1.40	0.06	1.44
1995ay	0.480	1.480	1.36	0.12	1.45
1996cg	0.490	1.490	1.58	0.07	1.46
1996ci	0.495	1.495	1.53	0.07	1.47
1995as	0.498	1.498	1.64	0.16	1.47
1997H	0.526	1.526	1.38	0.08	1.50
1997L	0.550	1.550	1.51	0.14	1.52

Continued next page

TABLE A8 (Continued)
Observed Widths of Type Ia Supernovae
Light Curves from Goldhaber

SNs	z	(1 + z)	w	σ(w)	Regr w
	Data	Calc	Data	Data	
1996cf	0.570	1.570	1.61	0.11	1.54
1997af	0.579	1.579	1.39	0.08	1.55
1997F	0.580	1.580	1.62	0.11	1.55
1997aj	0.581	1.581	1.49	0.09	1.55
1997K	0.592	1.592	1.87	0.30	1.56
1997S	0.612	1.612	1.90	0.10	1.58
1995ax	0.615	1.615	1.88	0.18	1.58
1997J	0.619	1.619	1.63	0.21	1.59
1995at	0.655	1.655	1.84	0.12	1.62
1996ck	0.656	1.656	1.51	0.20	1.62
1997R	0.657	1.657	1.65	0.12	1.62

Outliers